THE ASTROPHYSICAL JOURNAL, 325:725–748, 1988 February 15

NONRADIAL OSCILLATIONS OF NEUTRON STARS

P. N. McDERMOTT
Department of Physics and Astronomy, Northwestern University
H. M. VAN HORN
Department of Physics and Astronomy, C. E. Kenneth Mees Observatory, and Laboratory for Laser Energetics, University of Rochester
AND
C. J. HANSEN
Department of Astrophysical, Planetary, and Atmospheric Sciences, University of Colorado
Received 1987 June 11; accepted 1987 August 4

ABSTRACT

Finite-temperature neutron star models with a fluid core, solid crust, and thin surface fluid "ocean" are capable of sustaining a broad diversity of normal modes of oscillation. We have performed linear, adiabatic, Newtonian, nonradial pulsation analyses of such stars, including the elastic effects of the neutron star crust.

For any star, there are two general categories of nonradial oscillations: spheroidal modes and toroidal modes. The spheroidal modes, in turn, are comprised of several subclasses. The *p*-, *f*-, and *g*-modes are well known from conventional stellar pulsation theory. For neutron stars, two additional classes of modes that we term *s*- and *i*-modes result from crustal elasticity and are relatively new to stellar astrophysics. The *f*- and *p*-modes have periods of a few tenths of milliseconds, with higher overtones having shorter periods. There are two groups of *g*-modes. The core *g*-mode displacements are confined almost completely to the fluid core, while the surface *g*-modes are limited primarily to the thin fluid layer overlying the crust. The core *g*-modes have quadrupole ($l = 2$) periods $\Pi_g^c \gtrsim 10$ s, and the surface *g*-modes have quadrupole periods $\Pi_g^s \gtrsim 50$ ms, both for $T_c \lesssim 10^8$ K. The *g*-mode periods are roughly inversely proportional to the internal temperature T_c. The *s*-modes are essentially normal modes of shear waves in the solid neutron star crust. These modes have quadrupole periods $\Pi_s \lesssim 1$ ms and depend strongly on the crust thickness. Waves can also propagate on the solid-fluid interfaces, and the normal modes corresponding to such waves are the interfacial (*i*-) modes. The periods of these modes depend strongly on the local density and temperature at the interfaces.

In the absence of rotation and magnetic fields, the toroidal oscillations of neutron stars consist of a single subclass: the torsional oscillations, which are normal modes of elastic waves in the solid crust. The fundamental torsional mode has a quadrupole period of ~ 20 ms and is remarkably independent of the stellar mass. The overtones have shorter periods $\Pi_{tn} \approx 2$ ms $\Delta r/n$, where n is the overtone number, and Δr is the crustal thickness in kilometers.

Damping mechanisms we have investigated include gravitational radiation damping, neutrino emission damping, electromagnetic radiation from an oscillating stellar magnetic field, nonadiabatic effects, and internal friction and viscosity. Which of these mechanisms dominates depends upon the type of mode, the spherical harmonic index l, the equilibrium model, and other parameters.

Finally, we suggest that surface *g*-modes may be excited during thermonuclear outbursts in X-ray bursters and may lead to observable quasi-periodic oscillations.

Subject headings: pulsars — stars: interiors — stars: neutron — stars: pulsation

I. INTRODUCTION

a) Observational Motivation

Two disparate types of observations are suggestive of nonradial oscillations in neutron stars. The drifting subpulses and micropulses detected in some radio pulsars provide one example. The other is the quasi-periodic variability seen in some X-ray burst sources, as well as the quasi-periodic oscillations (QPOs) recently discovered in a number of bright X-ray sources (Lewin and van Paradijs 1986).

i) *Pulsars*

Individual pulses in radio pulsars are often composed of one or more subpulses having characteristic widths of 3–10 degrees of longitude (Manchester and Taylor 1977; Smith 1977). In some pulsars the subpulses drift systematically through the integrated pulse profile, with a separation time P_2 between successive subpulses ranging from 10 to 50 ms (Manchester and Taylor 1977; Wright and Fowler 1981). The drift band spacing P_3 is the time between subpulses at a fixed phase (see Fig. 5 of Taylor and Manchester 1977) and ranges from 10^0 to 10^2 s (Cordes 1981).

Microstructure, consisting of short duration (0.1 ms) spikes, has been observed in ~ 12 pulsars. These micropulses are often quasi-periodic, with periods ranging from $P_\mu \sim 0.1$ to 5 ms (Cordes 1981, and references therein) and are of low Q, varying on time scales of ~ 10 ms (Cordes 1976). Boriakoff (1976) first proposed that the 0.9 ms quasi-periodicity he detected in the microstructure of PSR 2016+28 might be due to neutron star oscillations. Van Horn (1980) elaborated upon this proposal by suggesting that the micropulse periodicities might be due either to $l = 0$ or to $l = 1$ *p*-modes of the neutron star and that the subpulse-to-subpulse variations might be caused by beating of *p*-modes closely spaced in period.

Van Horn (1980) also suggested a possible association of subpulses ($P_2 \sim 10$–50 ms) with torsional oscillations of the neutron star. This suggestion contains the possibility of a simple explanation of the subpulse drift phenomenon. In a rotating star, the nonradial oscillation frequencies are split into closely spaced multiplets, analogous to Zeeman splitting in atomic physics. The difference in frequency between rotationally split modes may correspond to the drift band spacing P_3.

Clearly, the drifting subpulses and micropulses represent complex phenomena which at present are not well understood. In addition, there are complications in connecting any postulated neutron star oscillations with observations of real pulsars. For example, any oscillation must be observed through the pulse window. This severely limits the number of pulses that can be observed and broadens the pulse width. Also the oscillations are passed through the pulsar emission mechanism, which is a noisy and as yet poorly understood process (see Ruderman and Sutherland 1975; Arons 1983, and references therein; Jones 1981, 1982, 1984). Further, many of the computed neutron star oscillation modes have periods which are longer than the pulsar rotation period. Rotational effects will thus be important for these modes, and such effects have not yet been treated. Pulsars typically also have magnetic field strengths $B \sim 10^{12}$ G. Carroll *et al.* (1986) have recently shown that such large fields strongly alter those modes concentrated near the neutron star surface, further complicating identifications with observed short time scale behavior in pulsars.

ii) *X-Ray Burst Sources*

The properties of X-ray burst sources have recently been reviewed by Lewin and Joss (1984) and by Joss and Rappaport (1984), and the outbursts are believed to be produced by explosive thermonuclear burning of matter accreted onto the surface of a neutron star.

In a number of X-ray burst sources and in several X-ray transient sources, periodicities ranging from ~ 10 to 70 ms have been observed (see Livio and Bath 1982; Livio 1982; Sadeh and Livio 1982). Livio and Bath (1982) in particular have reviewed several possible models for the origin of these phenomena and have concluded that g-mode oscillations of the neutron star are the most promising candidates. Very recent calculations by McDermott and Taam (1985, 1987) strongly suggest that the $l = 1$ g-mode, with minimum period ~ 12 ms, may be directly excited in the outermost surface layers due to the ϵ-mechanism associated with rapid alpha captures.

b) *Prior Theory*

i) *Overview of the Neutron Star Oscillation Spectrum*

A general stellar model can sustain two main classes of nonradial oscillations: spheroidal modes and toroidal modes. For a neutron star with a fluid core, solid crust, and surface fluid "ocean" of molten crustal material (a configuration we term a "three-component" neutron star), the spheroidal oscillations consist of several different subclasses: p-modes, g-modes, an f-mode, and modes new to stellar pulsation theory that we have named s- and i-modes. The p-modes are essentially normal modes corresponding to acoustic waves, and their properties are sensitive to the mean density of the neutron star. The period of a p-mode can be estimated as the travel time of an acoustic wave across the star. This yields a period $\Pi_p \sim R_*/c_l \sim 10^6$ cm/10^{10} cm s$^{-1} \sim 0.1$ ms. The g-modes result from the thermally induced buoyancy of perturbed elements of matter. Estimates of the g-mode periods are more difficult than for the p-modes, because the mode properties are very sensitive to the thermal properties of the equilibrium model. The g-modes and the p-modes are separated by a single f-mode for each $l \geq 2$. The period of the f-mode is close to, but slightly longer than, that of the fundamental p-mode. The s- and t-modes are, respectively, spheroidal and toroidal shear-dominated modes. The periods of these modes can be estimated as the time required for a shear wave to cross the crust of a typical neutron star. For a crust thickness of 2 km and a shear speed $c_t \sim 10^8$ cm s^{-1}, we obtain a period ~ 2 ms. The i-modes are interfacial modes concentrated at the fluid/solid interfaces in the neutron star. The periods of these modes depend very sensitively upon conditions near the interfaces.

ii) *Spheroidal Oscillations of Zero-Temperature Models*

The detailed general relativistic theory of nonradial stellar pulsations was first developed in a series of pioneering papers by Thorne and his coworkers (Thorne and Campolattaro 1967; Thorne 1969; Campolattaro and Thorne 1970; Ipser and Thorne 1973). The most recent addition to this literature is the paper by Lindblom and Detweiler (1983), which contains a comprehensive study of the quadrupole f-modes for models based on 13 different equations of state. The mode periods were found to lie between ~ 0.1 to 1 ms for a broad range of central densities and for a diverse set of equations of state. Gravitational wave damping times were found to be typically a few tenths of a second.

Although the present paper is confined to a study of nonradial oscillations, it seems appropriate also to mention briefly the previous work on radial oscillations, which comprise a special case corresponding to $l = 0$. Such modes have been studied in some detail by Meltzer and Thorne (1966), by Bardeen, Thorne, and Meltzer (1966), and more recently by Glass and Lindblom (1983). Glass and Lindblom have computed the fundamental and first-overtone radial pulsation modes for neutron star models constructed from 13 different equations of state and have found periods of a few tenths of a millisecond, of the same magnitude as nonradial acoustic modes.

iii) *Toroidal Oscillations of Zero-Temperature Models*

Toroidal oscillations are less familiar than spheroidal modes in stellar pulsation theory because they are generally all degenerate at zero frequency. Restoring forces provided by rotation, magnetic fields, or nonzero shear modulus break this degeneracy. In a neutron star with a solid crust, these modes, also called torsional oscillations, thus have finite periods. Torsional oscillations of neutron stars were first considered qualitatively by Ruderman (1968). Hansen and Cioffi (1980) carried out the first detailed numerical computations, using Newtonian pulsation theory. These calculations yielded fundamental toroidal mode periods of ~ 20 ms, with the period being remarkably independent of stellar mass. Overtones have periods $\lesssim 2$ ms. Recently the relativistic theory of toroidal oscillations has been developed in a comprehensive paper by Schumaker and Thorne (1983). Because toroidal oscillations have zero Lagrangian density variations (i.e., $\delta\rho = 0$), they have no time-varying mass quadrupole moment, and gravitational radiation is produced only by higher order processes. The gravitational radiation damping times for these modes are accordingly very long; Schumaker and Thorne estimate 10^4 yr for the quadrupole modes.

iv) *Finite-Temperature Models*

In homogeneous, zero-temperature stars, all g-mode frequencies are zero. Either strong material discontinuities or finite temperatures can break this degeneracy. McDermott, Van Horn, and Scholl (1983) carried out the first computations of g-modes in neutron star models with nonzero temperature, treating the star as a wholly fluid body (i.e., ignoring the nonzero shear stength of the crust). They found $\Pi_g \gtrsim 50$ ms for a model with central temperature $\sim 10^8$ K and showed that the g-mode periods vary approximately as the inverse of the central temperature. These modes have significant amplitude only in the outermost few meters of the neutron star, and they are only weakly damped by gravitational radiation, with damping times in the cooler neutron star models exceeding the Hubble time.

Very recently, Finn (1987) has investigated the effect of density discontinuities associated with abrupt changes in nuclear equilibrium composition in zero-temperature models, using a "slow motion" general relativistic formalism. He finds discontinuity g-modes associated with these interfaces.

The effects of a solid crust upon the spheroidal oscillation spectrum of a neutron star were first included in the work of McDermott (1985). A preliminary report of these results was presented by McDermott *et al.* (1985), and the present work contains a detailed account of these calculations. These results are based upon the Newtonian theory of elastodynamics. At the time these calculations were done, the general relativistic pulsation equations for spheroidal oscillations of models with nonzero shear modulus had not yet been derived. This situation has now been rectified by Finn (1987), but the Newtonian theory is sufficient for the purposes of this survey of the general properties of the oscillation modes.

c) *Structure of Paper*

Realistic neutron star models are capable of sustaining a wide variety of normal modes of oscillation. In this paper we describe the oscillation spectra of nonrotating, nonmagnetic neutron stars, using a linearized adiabatic analysis that includes the effects of the crustal elasticity. More detail can be found in McDermott (1985). The equilibrium configuration is a "three-component" model consisting of a fluid core, a solid crust, and a thin surface fluid layer we term the "ocean."

The plan of this paper is as follows. The equilibrium models are first briefly discussed in § II. In § III we derive the (Newtonian) pulsation equations, including boundary and interfacial "jump" conditions. A local analysis of the pulsation equations is carried out in § IV in order to provide a background for the detailed numerical calculations. The numerical results for the spheroidal mode spectrum are discussed in § V, and the comparable results for the toroidal modes are discussed in § VI. Various possible damping mechanisms for the nonradial oscillation modes are discussed in § VII, and in § VIII we conclude with a summary and discussion of our principal conclusions. The numerical method used to solve the equation set for stellar models with internal boundaries is described in the Appendix.

II. EQUILIBRIUM MODELS

Realistic three-component neutron star models were made available to us from the neutron star evolutionary cooling calculations of Richardson (1980; see also Richardson *et al.* 1982), and these have formed the foundation for the present investigation.

Richardson (1980) computed two sequences of fully general relativistic, quasi-static evolutionary models for cooling neutron stars. These calculations provide detailed numerical solutions of the evolutionary equations given by Thorne (1977). In one sequence, the stellar mass was chosen to be 0.503 $M_\odot$, and in the second, 1.33 $M_\odot$. In both sets of models, the material properties of the neutron star matter were assumed to have the following characteristics. The outer crust, extending down to the neutron drip point at $\rho = 4.3 \times 10^{11}$ g cm^{-3}, was assumed to consist of bare Fe nuclei embedded in a uniform, neutralizing, degenerate electron gas, which becomes relativistic for densities $\rho \gtrsim 10^6$ g cm^{-3}. In addition to the thermodynamic contributions from the nuclear and electronic kinetic energies, the equation of state employed included contributions from photons, from the Coulomb interactions between nuclei and electrons, and from nuclear vibrations and rotations.

Throughout the envelope of a neutron star, the Coulomb interaction between ions is strong. The strength of this interaction is characterized by the dimensionless parameter Γ, which is the ratio of the Coulomb energy to kT (see Brush, Sahlin, and Teller 1966). The matter of the outer crust undergoes a first-order fluid/solid phase transition at the position where $\Gamma = 155$. At a temperature of 10^9 K, this corresponds to a density $\rho \sim 5 \times 10^{10}$ g cm^{-3}. Thus, for Richardson's evolutionary sequences, which span the range of central temperatures from 10^9 to 10^7 K, the crystallization boundary marking the crust/ocean interface always occurs closer to the surface of the star than the neutron drip point.

An important quantity for our calculations is the shear modulus of the solid lattice. The prescription we have used to compute this is that given by Pandharipande, Pines, and Smith (1976):

$$\mu = 0.3711 \frac{Z^2 e^2 n_N^{4/3}}{2^{1/3}}, \quad (1)$$

where n_N is the number density of the nuclei. It is noteworthy that the shear speed $c_t = \mu/\rho \sim 10^8$ cm/s is remarkably constant throughout the neutron star crust, as previously noted by Ruderman (1968).

The inner crust of the neutron star, which we take to be the region of densities between the neutron drip point at $\rho = 4.3 \times 10^{11}$ g cm^{-3} and the base of the crust at 2.4×10^{14} g cm^{-3}, is assumed to consist of nuclei with $Z \approx 40$, degenerate, relativistic electrons, and degenerate, nonrelativistic neutrons. The actual composition of the nuclei in the inner crust is taken from the work of Negele (1974) and of Negele and Vautherin (1973), who also give the zero-temperature equation of state for such matter. In addition to the zero-temperature thermodynamic properties, the equation of state used included the leading thermal corrections for the nuclei, electrons, and free neutrons. For the nuclei and electrons, these properties were computed as for the outer crust, while the thermal properties of the free neutrons were taken to be those of an ideal, noninteracting Fermi gas, modified to take account of superfluidity as discussed by Yang and Clark (1971) and Muhlschlegel (1959). The effect of neutron superfluidity is to reduce the contribution of these particles to the heat capacity and to suppress the neutrino emission from the modified URCA nucleon-nucleon bremsstrahlung process (Maxwell 1978; Friman and Maxwell

TABLE 1

NEUTRON STAR MODELS

Model	Mass ($M_\odot$)	T_c (K)	R_* (km)	ρ_c (g cm^{-3})	d (cm)	Δt_{cr} (km)	ρ_0 (g cm^{-3})
Fiducial	0.503	1.03+7	10.1	9.44+14	1.80+2	2.45	1.04+5
NS05T7	0.503	1.03+7	9.839	9.44+14	3.71+1	2.36	5.23+4
NS05T8	0.503	9.76+7	9.785	9.44+14	2.86+4	2.02	2.76+10
NS13T8	1.326	1.05+8	7.853	3.63+15	1.75+3	0.41	4.24+9

1979). The neutrons are superfluid from approximately the point of neutron drip to a density of $\sim 1 \times 10^{14}$ g cm^{-3}.

At densities greater than 2.4×10^{14} g cm^{-3}, the lattice is assumed to dissolve, and the core of the neutron star is taken to consist of a mixture of free and highly degenerate neutrons, protons, and electrons. The equation of state of zero-temperature matter in this regime is taken to be that given by Baym, Bethe, and Pethick (1971), extended to the highest densities by Pandharipande, as quoted by Baym, Pethick, and Sutherland (1971). To this zero-temperature equation of state are added the leading thermal corrections for the three species, computed as for noninteracting particles and modified for neutron and proton superfluidity as discussed above. The nucleons are superfluid over essentially the entire core. At densities above $\rho = 5 \times 10^{14}$ g cm^{-3}, the models are assumed to contain a pion condensate (see Scalapino 1972). The contributions of these particles to the material properties are negligible, except that they strongly enhance the neutrino emission rate and thus greatly accelerate the cooling of the neutron star. We note that, while the equilibrium neutron star models explicitly include the effects of superfluidity of the neutrons and protons, the pulsation calculations we have performed have not taken this into account but have simply treated the neutrons and protons as ordinary fluids. Thus, in particular, we are unable to discuss Tkachenko oscillations of the superfluid vortex lines (Ruderman 1970).

a) *Fiducial Model*

We have selected a 0.5 $M_\odot$ neutron star model with $T_c = 1.03 \times 10^7$ K from the evolutionary sequence computed by Richardson (1980; see also Richardson *et al.* 1982) as a fiducial model for our nonradial pulsation calculations. Most of our code development has been carried out using this model, and we report the results of our computations in some detail. McDermott, Van Horn, and Scholl (1983) also have studied the pulsations of this model, approximating it as a completely fluid star, and we have also used it to perform preliminary calculations for a neutron star with a fluid core, solid crust, and a surface fluid ocean. The surface layers of this model, however, are approximated as a polytropic ideal gas of fully ionized iron. This does not represent the microphysics well enough to yield reliable results for those modes which have largest amplitudes near the neutron star surface. For this reason, the results for the fiducial model are primarily of academic interest, and our results of more physical interest are those obtained for the composite models described below.

b) *Composite Models*

The equilibrium neutron star models used in most of our pulsation calculations are composites of Richardson's evolutionary cores, to which are appended detailed neutron star envelopes constructed by Gudmundsson (1981; see also Gudmundsson *et al.* 1983). Clearly, a perfect match of core and envelope is not possible, and we have contented ourselves with requiring continuity of the pressure, temperature, radius, baryon number, and gravitational potential at the matching point, taken to be at mass density $\rho \approx 10^{10}$ g cm^{-3}. The luminosity, however, has a substantial discontinuity. This does not affect the qualitative results of the present, adiabatic calculations, although quantitative values for those pulsation modes which are more sensitive to the thermal structures of the models may be somewhat modified. Nonadiabatic calculations can be expected to be quite seriously affected, however, and we have avoided all but the most general of such computations for this reason.

We have constructed three composite models in the manner described above. Two have mass $M_* = 0.503\ M_\odot$. One of these, at age 0.47 yr, has central temperature $T_c = 9.76 \times 10^7$ K; this model is designated "NS05T8." The second model, representing a later evolutionary stage at 155 yr, has $T_c = 1.03 \times 10^7$ K, and it is designated "NS05T7." The remaining model, from a different evolutionary sequence, has mass $M_* = 1.33\ M_\odot$, $T_c = 1.05 \times 10^8$ K, and age 0.035 yr; this model we designate "NS13T8." The properties of these composite models, as well as those of the fiducial model, are summarized in Table 1. Besides M_* and T_c, this table contains the stellar radius R_*, the central density ρ_c, the depth d of the surface fluid "ocean," the thickness Δt_{cr} of the solid crust, and, finally, the density ρ_0 at the base of the ocean. For a more detailed description of the characteristics of the composite models, see McDermott (1985).

III. PULSATION EQUATIONS

a) *General Form*

The calculations described in McDermott, Van Horn, and Scholl (1983) are based upon a relativistic version of the Cowling approximation, in which all perturbations to the metric tensor are neglected. In the nonrelativistic limit, these equations reduce directly to the Newtonian fluid Cowling equations, which we now describe.

In the presence of solid matter, the hydrodynamic equations normally used in stellar pulsation theory must be generalized to allow for shearing stresses that an inviscid fluid cannot support. The pulsation equations for nonradial oscillations with nonzero shear modulus are derived in an astrophysical context by Van Horn and Savedoff (1976) and were first applied to white dwarfs with crystalline cores by Hansen and Van Horn (1979). There is also a wealth of geophysical literature on the subject of normal modes of self-gravitating spheres which provides very helpful guidance, and we have found the books by Lapwood and Usami (1981) snd by Aki and Richards (1980) and the paper by Alterman, Jarosch, and Pekeris (1959) to be particularly useful. The application of the theory to the free oscillations of the Earth (Buland 1981) has been very successful in revealing details about the interior of

our planet, and one may hope that eventually the study of neutron star oscillations will prove similarly successful in providing information about the interiors of these extremely dense stars.

The deformation of a solid body is described by the Lagrangian displacements $\boldsymbol{u}(\boldsymbol{x}, t)$ of infinitesimal mass elements from their equilibrium positions. It is useful to define a strain tensor u_{ik} (see Landau and Lifshitz 1970), which for small deformations is given by

$$u_{ik} = \frac{1}{2}\left(\frac{\partial u_i}{\partial x_k} + \frac{\partial u_k}{\partial x_i}\right) = u_{ki} . \tag{2}$$

If the strain tensor is diagonalized at a point, the diagonal components represent the fractional change in the length along the principal axes at that point. For example, u_{xx} is the fractional change in distance between two elements lying on the x-axis. The trace, u_{ii}, of the strain tensor is the fractional change in volume of a small volume element V due to the deformation.[1] That is $u_{ii} = \delta V/V = -\delta\rho/\rho$, where δV and $\delta\rho$ are the changes in volume and density during the deformation.

The equations governing the motion of a mass element are the continuity equation, the momentum equation, and Poisson's equation:

$$\frac{\partial \rho}{\partial t} + \nabla \cdot (\rho \boldsymbol{v}) = 0 , \tag{3a}$$

$$\frac{\partial \boldsymbol{v}}{\partial t} + (\boldsymbol{v} \cdot \nabla)\boldsymbol{v} = \frac{1}{\rho}\nabla \cdot \boldsymbol{\sigma} - \nabla\Phi , \tag{3b}$$

$$\nabla^2\Phi = 4\pi G\rho , \tag{3c}$$

where $\partial\sigma_{ij}/\partial x_j$ is the ith component of the divergence of the stress tensor σ_{ij}.

To derive pulsation equations, we apply perturbations to these equations and the equations describing the behavior of the elastic solid and retain only terms of first order in the perturbation variables (see Cox 1980 or Unno *et al.* 1979 for this procedure applied to the equations of fluid dynamics; Van Horn and Savedoff 1976 and Hansen and Van Horn 1979 give the corresponding results for an elastic solid.). As usual, we use primes to denote Eulerian perturbations and δ to denote Lagrangian perturbations (moving with the mass element). We assume the unperturbed state to be one of hydrostatic equilibrium, so that the unperturbed velocity $\boldsymbol{v}_0 = 0$. If f represents a typical perturbation variable, we have in this approximation $df/dt = \partial f/\partial t + (\boldsymbol{v} \cdot \nabla)f \approx \partial f/\partial t$. In particular, the Lagrangian perturbation velocity $\boldsymbol{v}$ is given by

$$\boldsymbol{v} = \frac{\partial \boldsymbol{u}}{\partial t} + (\boldsymbol{v}_0 \cdot \nabla)\boldsymbol{u} \approx \frac{\partial \boldsymbol{u}}{\partial t} . \tag{4}$$

The deformation of a solid produces internal forces described in terms of the stress tensor $\sigma_{ik} = \sigma_{ki}$, which is a measure of the internal force per unit area. The stress tensor σ_{ik} can be interpreted as the ith component of the force acting on a unit area oriented perpendicular to the x_k-axis. In the special case of an inviscid fluid, $\sigma_{ik} = -p\delta_{ik}$, where p is the pressure. It also turns out to be useful often to refer to the traction $\boldsymbol{t}$, which is the force per unit area acting across an internal surface. If $\boldsymbol{n}$ is the unit normal vector to such a surface, the traction is $t_i = n_j\sigma_{ji}$.

[1] We use the summation convention throughout, unless otherwise noted: repeated indices denote summation over all values.

It should be observed that the equilibrium state of a star is much different from the equilibrium state normally considered. Typically, in standard elasticity theory, the equilibrium state is one in which the stress and strain are zero. For a star in hydrostatic equilibrium, the stresses $-p\delta_{ik}$ are extremely large. If a state of zero stress and strain could somehow be postulated for stellar material, then one would be forced into the realm of nonlinear stress-strain theory. Instead, the approach we adopt is the one used by previous workers in both astrophysics and geophysics. This is to define the initial strain as zero in the reference (hydrostatic equilibrium) state and to take the initial stress as $\sigma_{ik}^{(0)} = -p^{(0)}\delta_{ik}$. The perturbations are then small strains that are studied in relation to the small incremental stresses they produce. The problem of initial stress is not trivial and is discussed by Aki and Richards (1980, and references therein).

For adiabatic motion in an isotropic elastic solid, the relationship between the incremental stress $\delta\sigma_{ik}$ and the strain is

$$\delta\sigma_{ik} = (\Gamma_1 p u_{ll})\delta_{ik} + 2\mu(u_{ik} - \tfrac{1}{3}u_{ll}\delta_{ik}) , \tag{5}$$

where $\Gamma_1 \equiv (\partial \ln p/\partial \ln \rho)_s$, and the elasticity of the solid is measured by the shear modulus μ; see McDermott (1985, Appendix A), Aki and Richards (1980), or Van Horn and Savedoff (1976) for derivations of equation (5). When $\mu \to 0$, the perturbed stress tensor reduces to $\delta\sigma_{ik} \to \Gamma_1 p u_{ll}\delta_{ik} = -\Gamma_1 p(\delta\rho/\rho)\delta_{ik} = -\delta p_{ad}\,\delta_{ik}$, which is the adiabatic Lagrangian perturbation for an inviscid fluid.

A linear, adiabatic wave equation can be derived from the perturbed equations by assuming an oscillatory time dependence of the form $\boldsymbol{u}(\boldsymbol{x}, t) = \boldsymbol{\xi}(\boldsymbol{x})e^{i\sigma t}$, where σ is the pulsation frequency (see McDermott 1985 for details). The result is

$$\begin{aligned}\sigma^2\boldsymbol{u} = &-\nabla\left(\frac{\Gamma_1 p_0}{\rho_0}\nabla \cdot \boldsymbol{u}\right) - \nabla\left(\frac{1}{\rho_0}\boldsymbol{u} \cdot \nabla p_0\right) \\ &-\mathbf{1}_r A\frac{\Gamma_1 p_0}{\rho_0}\nabla \cdot \boldsymbol{u} + \nabla\Phi' + \frac{1}{\rho_0}\{\nabla(\tfrac{2}{3}\mu\nabla \cdot \boldsymbol{u}) - (\nabla\mu \cdot \nabla)\boldsymbol{u} \\ &-\nabla(\boldsymbol{u} \cdot \nabla\mu) + (\boldsymbol{u} \cdot \nabla)\nabla\mu - \mu[\nabla^2\boldsymbol{u} + \nabla(\nabla \cdot \boldsymbol{u})]\} ,\end{aligned} \tag{6}$$

where $\mathbf{1}_r$ is the unit vector in the radial direction, and A is defined by

$$A \equiv \frac{1}{\rho_0}\frac{d\rho_0}{dr} - \frac{1}{\Gamma_1 p_0}\frac{dp_0}{dr} . \tag{7}$$

The perturbation to the gravitational potential is given by

$$\nabla^2\Phi' = -4\pi G(\boldsymbol{u} \cdot \nabla\rho_0 + \rho_0\nabla \cdot \boldsymbol{u}) . \tag{8}$$

Equation (6) is the linear, adiabatic wave equation for nonradial oscillations of an elastic sphere. In the following subsections, we show how the angular dependence of this equation can be separated in two different ways, leading to the radial equations for the spheroidal and toroidal oscillation modes. From this point we drop the zero subscript on the equilibrium quantities.

b) Spheroidal Modes

The spheroidal separation of variables for the pulsation equations (6) and (8) is given by

$$\xi_r = U(r)Y_{lm} , \qquad \xi_\theta = V(r)\frac{\partial Y_{lm}}{\partial\theta} , \qquad \xi_\phi = \frac{V(r)}{\sin\theta}\frac{\partial Y_{lm}}{\partial\phi} , \tag{9a}$$

$$\Phi' = \hat{\Phi}'(r)Y_{lm} , \tag{9b}$$

where $Y_{lm}(\theta, \phi)$ are the usual spherical harmonics (see Jackson 1975). When these forms are inserted into equations (6) and (8), the pulsation equations become

$$\rho\sigma^2 U = \rho\frac{d\hat{\chi}}{dr} - A\Gamma_1 p\hat{\alpha} - \frac{d}{dr}\left(\frac{1}{3}\mu\hat{\alpha}\right) + \frac{d\mu}{dr}\left(\hat{\alpha} - 2\frac{dU}{dr}\right) - \mu\left[\frac{1}{r^2}\frac{d}{dr}\left(r^2\frac{dU}{dr}\right) - \frac{l(l+1)}{r^2}U + \frac{2l(l+1)}{r^2}V\right], \quad (10a)$$

$$\rho\sigma^2 V = \rho\frac{\hat{\chi}}{r} - \frac{1}{3}\frac{\mu\hat{\alpha}}{r} - \frac{d\mu}{dr}\left(\frac{dV}{dr} - \frac{V}{r} + \frac{U}{r}\right) - \mu\left[\frac{1}{r^2}\frac{d}{dr}\left(r^2\frac{dV}{dr}\right) - \frac{l(l+1)}{r^2}V + \frac{2}{r^2}U\right], \quad (10b)$$

$$\frac{1}{r^2}\frac{d}{dr}\left(r^2\frac{d\hat{\Phi}'}{dr}\right) - \frac{l(l+1)}{r^2}\hat{\Phi}' = 4\pi G\left(U\frac{d\rho}{dr} + \hat{\alpha}\rho\right), \quad (10c)$$

where

$$\hat{\alpha} = \frac{1}{r^2}\frac{d}{dr}(r^2U) - \frac{l(l+1)}{r}V, \quad (10d)$$

$$\hat{\chi} = -\frac{\Gamma_1 p}{\rho}\hat{\alpha} - \frac{1}{\rho}\frac{d\rho}{dr}U + \hat{\Phi}'. \quad (10e)$$

These equations are the same as those given by Van Horn and Savedoff (1976) or, with $\Phi' = 0$, those of Hansen and Van Horn (1979).

In general, stellar pulsations cause perturbations of the gravitational potential. Cowling (1941) showed that the basic features of nonradial oscillations can be obtained with reasonable accuracy even when Φ' is neglected. This "Cowling approximation" reduces the order of the system of differential equations (eqs. [10a]–[10e]) by two, considerably simplifying the calculations. All of the calculations we report in the present work are based on this approximation, but we note here that it may eventually prove inadequate for modes formed deep within the star.

In the core and ocean of the neutron star matter is in a fluid state, while in the crust it, of course, is solid. Equations (10a)–(10e), which are written for a solid, can easily be shown to reduce to the corresponding fluid equations as $\mu \to 0$. To solve the global pulsation problem for the three-component models, the equations appropriate to the solid crust must be solved simultaneously with the fluid equations appropriate to the ocean and core, with the solutions coupled together at the ocean/crust and crust/core interfaces by suitable "jump" conditions. The forms of these interfacial boundary conditions are given explicitly in the following subsection.

For the solid crust it is convenient to recast equations (10a)–(10c) in the form of four first-order ordinary differential equations written in terms of suitable dimensionless variables. We use the quantities

$$z_1 \equiv \frac{U}{r}, \quad z_2 \equiv \frac{1}{\rho}\left(\lambda\hat{\alpha} + 2\mu\frac{dU}{dr}\right), \quad z_3 \equiv \frac{V}{r}, \quad z_4 \equiv \frac{\mu}{p}\left(\frac{dV}{dr} - \frac{V}{r} + \frac{U}{r}\right), \quad (11)$$

where $\lambda \equiv \Gamma_1 p - 2/3\mu$ is the Lamé coefficient. These quantities are related to the variables used by Hansen and Van Horn (1979), but their definitions are slightly different than the ones we use here. The variables z_1 and z_3 are, respectively, the radial and transverse displacements in dimensionless form, while z_2 and z_4 are proportional to the radial and transverse tractions. The tractions appropriate to the spheroidal separation of variables are explicitly given by

$$\delta t_r = \left(\lambda\hat{\alpha} + 2\mu\frac{dU}{dr}\right)Y_{lm}e^{i\sigma t}, \quad (12a)$$

$$\delta t_\theta = \mu\left(\frac{dV}{dr} - \frac{V}{r} + \frac{U}{r}\right)\frac{\partial Y_{lm}}{\partial\theta}e^{i\sigma t}, \quad (12b)$$

$$\delta t_\phi = \mu\left(\frac{dV}{dr} - \frac{V}{r} + \frac{U}{r}\right)\frac{1}{\sin\theta}\frac{\partial Y_{lm}}{\partial\phi}e^{i\sigma t}. \quad (12c)$$

For numerical calculations, it is useful to introduce the new independent variable $x = \ln(r/p)$, which has the virtue of providing more uniform zoning. With this choice, and using the dimensionless variables introduced in equation 11, the spheroidal pulsation equations (eqs. [10a]–[10e]) become, in the Cowling approximation,

$$(1+\tilde{V})\frac{dz_1}{dx} = -\left(1 + 2\frac{\alpha_2}{\alpha_3}\right)z_1 + \frac{1}{\alpha_3}z_2 + l(l+1)\frac{\alpha_2}{\alpha_3}z_3, \quad (13a)$$

$$(1+\tilde{V})\frac{dz_2}{dx} = \left(-c_1\tilde{V}\Omega^2 - 4\tilde{V} + \tilde{U}\tilde{V} + 12\Gamma_1\frac{\alpha_1}{\alpha_3}\right)z_1 + \left(\tilde{V} - 4\frac{\alpha_1}{\alpha_3}\right)z_2 + l(l+1)\left(\tilde{V} - 6\Gamma_1\frac{\alpha_1}{\alpha_3}\right)z_3 + l(l+1)z_4, \quad (13b)$$

$$(1+\tilde{V})\frac{dz_3}{dx} = -z_1 + \frac{1}{\alpha_1}z_4, \quad (13c)$$

$$(1+\tilde{V})\frac{dz_4}{dx} = \left(\tilde{V} - 6\Gamma_1\frac{\alpha_1}{\alpha_3}\right)z_1 - \frac{\alpha_2}{\alpha_3}z_2 + \left[-c_1\tilde{V}\Omega^2 + \frac{2}{\alpha_3}\{[2l(l+1)-1]\alpha_1\alpha_2 + 2[(l(l+1)-1]\alpha_1^2\}\right]z_3 + (\tilde{V} - 3)z_4, \quad (13d)$$

where

$$\alpha_1 \equiv \frac{\mu}{p}, \quad \alpha_2 \equiv \Gamma_1 - \frac{2}{3}\frac{\mu}{p}, \quad \alpha_3 \equiv \Gamma_1 + \frac{4}{3}\frac{\mu}{p}, \quad (14)$$

and

$$\tilde{V} \equiv -\frac{d\ln p}{d\ln r} = \frac{\rho g r}{p}, \quad \tilde{U} \equiv \frac{d\ln M_r}{d\ln r}, \quad c_1 \equiv \left(\frac{r}{R_*}\right)^3\frac{M_*}{M_r}, \quad \Omega^2 \equiv \frac{\sigma^2 R_*^3}{GM_*}. \quad (15)$$

For the fluid pulsation problem, a different choice of dimensionless variables is necessary. The fluid problem is second order, as opposed to the fourth-order system defined by the pulsations of the solid crust. A convenient choice of variables for the fluid problem is the set of "Dziembowski variables" which have been widely used in computations of the nonradial

oscillations of stars (see Unno *et al.* 1979; Cox 1980):

$$y_1 \equiv \frac{U}{r}, \qquad y_2 \equiv \frac{p'}{\rho g r}. \tag{16}$$

These quantities are related to the dimensionless variables z_i through by the expressions

$$z_1 = y_1, \qquad z_2 = \tilde{V}(y_1 - y_2), \qquad z_3 = \frac{g}{\sigma^2 r} y_2. \tag{17}$$

Note that z_3 is no longer an independent quantity in the fluid case but is a linear combination of z_1 and z_2.

In terms of the Dziembowski variables, the fluid pulsation equations are given by

$$(1 + \tilde{V})\frac{dy_1}{dx} = \left(\frac{\tilde{V}}{\Gamma_1} - 3\right)y_1 + \left[\frac{l(l+1)}{c_1\Omega^2} - \frac{\tilde{V}}{\Gamma_1}\right]y_2, \tag{18a}$$

$$(1 + \tilde{V})\frac{dy_2}{dx} = (c_1\Omega^2 + Ar)y_1 + (1 - \tilde{U} - Ar)y_2. \tag{18b}$$

These are the forms we employ in the fluid ocean and core of the neutron star.

i) *Boundary Conditions*

The boundary condition at the center of the neutron star may be obtained by expanding y_1 and y_2 about the center and requiring that these variables be regular at $r = 0$. The result of this expansion is

$$\frac{c_1\Omega^2}{l} y_1 - y_2 = 0. \tag{19a}$$

The surface boundary condition is obtained by the requirement that $\delta p/p \to 0$ as $r \to R_*$. We carry out expansions valid near the stellar surface to obtain (see Carroll 1981)

$$(\tilde{V} - c_1\Omega^2 - 4 + \tilde{U})y_1 + \left[\frac{l(l+1)}{c_1\Omega^2} - \tilde{V}\right]y_2 = 0. \tag{19b}$$

Because the pulsation equations are linear, they do not fix the absolute amplitude of the oscillations. It is customary in stellar pulsation theory to establish the amplitude by normalizing the relative radial displacement to unity at the stellar surface:

$$y_1(R_*) = 1. \tag{19c}$$

We adopt this same convention.

To connect the eigenfunctions y_1 and y_2 for the fluid ocean and core to the eigenfunctions z_1–z_4 used in the solid crust, appropriate interfacial jump conditions must be employed. The physical conditions which must be satisfied at any interface are continuity of the radial displacement and of the tractions:

$$z_1 = y_1, \tag{20a}$$

$$z_2 = \tilde{V}(y_1 - y_2), \tag{20b}$$

$$z_4 = 0. \tag{20c}$$

Note that the horizontal traction (proportional to z_4) is identically zero in a fluid because an inviscid fluid cannot support shear stresses.

c) *Toroidal Modes*

The toroidal modes of a nonrotating, nonmagnetic neutron star are torsional oscillations, which are normal modes of shear waves in the solid crust. For $l = 1$, these modes are manifested as a simple oscillatory twisting of the crust. For this case, $\boldsymbol{u}$ can be written in the form $\boldsymbol{u} = \boldsymbol{\Omega} \times r e^{i\sigma t}$, where Ω is a general function of r (see Aizenman and Smeyers 1977). Illustrations of the velocity field for low-l toroidal oscillations are shown in Saio (1982).

The toroidal separation of variables is defined by the conditions

$$\nabla \cdot \boldsymbol{u} \equiv 0, \qquad u_r \equiv 0. \tag{21}$$

This immediately implies that $\delta\rho \equiv 0$ and $\Phi' \equiv 0$, from the perturbed forms of the continuity equation and Poisson's equation. Note that for any quantity f, $\delta f = f' + \boldsymbol{u} \cdot \nabla f = f'$, since f depends only on r in the equilibrium model. Thus Eulerian and Lagrangian perturbations are identical for toroidal oscillations.

In spherical coordinates, the separation of variables that satisfies conditions given in equation (21) is

$$u_\theta = W(r)\frac{1}{\sin\theta}\frac{\partial Y_{lm}}{\partial\phi} e^{i\sigma t}, \qquad u_\phi = -W(r)\frac{\partial Y_{lm}}{\partial\theta} e^{i\sigma t}. \tag{22}$$

Substitution of these expressions into the linear adiabatic wave equation (6) yields two identical equations for the pulsation amplitude W:

$$\sigma^2 W = \frac{\mu}{\rho}\left[-\frac{1}{\mu}\frac{d\mu}{dr}\left(\frac{dW}{dr} - \frac{W}{r}\right) - \frac{1}{r^2}\frac{d}{dr}\left(r^2\frac{dW}{dr}\right) + \frac{l(l+1)}{r^2} W\right]. \tag{23}$$

To solve this second-order equation numerically, we rewrite it as two first-order equations. To this end we introduce the two dimensionless variables S_1 and S_2:

$$S_1 \equiv \frac{W}{r}, \qquad S_2 \equiv \frac{\mu}{\sigma^2}\frac{R_*}{M_*}\left(\frac{dW}{dr} - \frac{W}{r}\right). \tag{24}$$

These quantities have the advantage of permitting us to avoid taking numerical derivatives of the poorly known quantity μ. They also have natural interpretations: S_1 is the dimensionless amplitude, and S_2 is proportional to the traction. In terms of these quantities, the system of equations for the toroidal modes becomes

$$r\frac{dS_1}{dr} = \frac{\sigma^2 M_*}{\mu R_*} S_2, \tag{25a}$$

$$r\frac{dS_2}{dr} = \frac{\mu R_*}{\sigma^2 M_*}\left[l(l+1) - 2 - \frac{\sigma^2\rho r^2}{\mu}\right]S_1 - 3S_2. \tag{25b}$$

i) *Boundary Conditions*

The boundary conditions for the toroidal oscillation modes are that the horizontal tractions must be zero at the top and bottom of the crust. In terms of the transverse amplitude W, the conditions $\delta t_\theta = \delta\sigma_{r\theta} = 0$ and $\delta t_\phi = \delta\sigma_{r\phi} = 0$ reduce to the single condition

$$\mu\left(\frac{dW}{dr} - \frac{W}{r}\right) = 0. \tag{26}$$

In terms of the dimensionless variable S_2, this condition is

$$S_2(r_i) = 0, \tag{27}$$

where r_i is the radius of either interface.

As in the case of the spheroidal oscillations, we require a normalization condition to complete the specification of the solution. With the vanishing of the tractions at the fluid/solid boundaries and with the radial displacement being identically zero for the toroidal modes, the pulsations of the crust completely decouple from the ocean and core. In consequence, we can no longer make use of the conventional normalization condition, viz. that the relative radial displacement equal unity at the stellar surface. Instead, for the toroidal modes we use the normalization condition that the relative *transverse* displacement be normalized to unity at the surface of the crust:

$$S_1(r_c) = 1 . \tag{28}$$

These conditions complete the definition of the eigenvalue problem for the toroidal oscillations.

IV. LOCAL ANALYSIS

Global solutions of the nonradial oscillation equations for a stellar model in general require numerical calculations. In the limit of very short wavelengths, however, the pulsation equations reduce to algebraic eigenvalue equations which can be solved analytically. This "local analysis" is useful in providing information about the nature of the pulsation modes in the short-wavelength limit and provides a guide to the detailed numerical calculations that follow.

Our starting point for a local analysis of the nonradial oscillations of neutron stars is the equation set (10a)–(10e), for spheroidal modes, or equation (23), for toroidal modes, with $\Phi' = 0$ in either case. When the wavelength associated with a perturbation is small compared to any characteristic length scale L of an equilibrium quantity, a perturbation variable can be written in the form:

$$f' = f_0 \exp(ikr) , \tag{29}$$

where $kr \gg 1, kL \gg 1$.

Under this condition, equations (10a)–(10e) yield

$$\sigma^2 U = \left[k^2 c_l^2 + ik\left(-\frac{2}{r} c_l^2 + g - A a_l^2 \right) + \frac{l(l+1)}{r^2} c_t^2 - A a_l^2 \frac{2}{r} \right] U + \frac{l(l+1)}{r} \times \left[ik(c_l^2 - c_t^2) - \frac{2}{r} c_t^2 + A a_l^2 \right] V , \tag{30a}$$

$$\sigma^2 V = \frac{1}{r} \left[-ik(c_l^2 - c_t^2) - \frac{2}{r} c_l^2 + g \right] U + \left[k^2 c_t^2 - ik \frac{2}{r} c_t^2 + \frac{l(l+1)}{r^2} c_l^2 \right] V . \tag{30b}$$

Here

$$a_l^2 \equiv \frac{\Gamma_1 p}{\rho} , \qquad c_l^2 \equiv a_l^2 + \frac{4}{3} \frac{\mu}{\rho} , \qquad c_t^2 \equiv \frac{\mu}{\rho} , \tag{30c}$$

where a_l is the speed of an acoustic wave in a fluid, and c_l and c_t are, respectively, the speed of a longitudinal and of a transverse wave in an isotropic, elastic solid.

Equations (30a)–(30c) comprise a second-order system in σ^2. One of the two roots of this dispersion relation is, to leading order in kr,

$$\sigma_+^2 \approx k^2 c_l^2 . \tag{31}$$

This root corresponds to shear-modified p-modes. In the fluid limit ($\mu \to 0$), this reduces to $\sigma_+^2 = k^2 a_l^2$, the usual dispersion relation for local acoustic waves.

The second root of equations (30a)–(30c) is, again to leading order in kr,

$$\sigma_-^2 \approx k^2 c_t^2 . \tag{32}$$

This root corresponds to shear waves in the neutron star crust. In the fluid limit, the character of this root totally changes. When $\mu \to 0$, the first nonvanishing terms yield

$$\lim_{\mu \to 0} \sigma_-^2 \approx \frac{l(l+1)}{(kr)^2} N^2 . \tag{33}$$

where $N^2 = -Ag$ is the square of the Brunt-Väisälä frequency. This is the usual dispersion relation for internal gravity waves.

From these limiting cases for the dispersion relations, we can obtain direct numerical estimates for the periods of the various global oscillation modes. For a low-order global mode, $kR_* \sim 1$. This stretches the limits of validity of the local approximation but leads to estimates which still are qualitatively correct.

For the p-modes, equation (31) yields for the estimated period

$$\Pi_p \approx \frac{0.5 \text{ ms}}{kR_*} \left(\frac{R_6^3}{M_*/M_\odot} \right)^{1/2} \approx \frac{0.5 \text{ ms}}{kR_*} \left(\frac{5 \times 10^{14} \text{ g cm}^{-3}}{\bar{\rho}} \right)^{1/2} , \tag{34}$$

where $R_6 = R_*/10^6$ cm.

The periods of the s-modes are conveniently estimated by using the fact that $c_t \sim 10^8$ cm s^{-1}, remarkably insensitive to depth in the neutron star crust. In terms of the crust thickness Δr, the period is approximately

$$\Pi_s \approx \frac{6 \text{ ms}}{k\Delta r} \frac{\Delta r}{1 \text{ km}} . \tag{35}$$

For the g-modes, equation (33) gives very different values for the surface layers and for the deep interior. To evaluate the periods for these modes, we use the following definitions (see Cox 1980):

$$A = H_p^{-1}(\chi_T/\chi_\rho)(\nabla - \nabla_{ad}) , \qquad H_p^{-1} \equiv -d \ln p/dr ,$$
$$\chi_T \equiv (\partial \ln p/\partial \ln T)\rho , \qquad \chi_\rho \equiv (\partial \ln p/\partial \ln \rho)_T ,$$
$$\nabla \equiv (d \ln T/d \ln p)_* , \qquad \nabla_{ad} \equiv (\partial \ln T/\partial \ln p)_s .$$

The periods of the surface g-modes are difficult to estimate *a priori* in any simple way (see McDermott, Van Horn, and Scholl 1983) because spatial gradients are extremely steep in these layers, and it is not possible to select "typical" values for the parameters. For the core g-modes, however, we may use values appropriate to an ideal neutron gas to obtain: $\chi_T \approx (5/6)\pi^2(kT/\epsilon_F)^2 \sim 10^{-9} T_7^2 R_6^4 (M_*/M_\odot)^{-4/3}$, $\chi_\rho \sim 5/3$, $\nabla_{ad} \sim 0.4$, and $\nabla \approx 0$. These values lead to

$$\Pi_g^c \approx 35 \text{ s} \frac{kR_*}{[l(l+1)]^{1/2}} T_7^{-1} R_6^{-1/2} \left(\frac{M_*}{M_\odot} \right)^{1/6} , \tag{36}$$

where $T_7 = T/10^7$ K.

Equations (30a)–(30c) also provide some information about the relations between the radial and transverse displacement eigenfunctions U and V. For the root σ_+^2, equation (30b) shows that $|U/V| \sim kr \gg 1$. Thus, in the local approximation,

mass motions in the p-modes are primarily radial. Conversely, for the shear modes (σ_-^2), equation (30a) shows that $|U/V| \sim l(l+1)/kr \ll 1$. Mass motions in the shear modes therefore are mainly transverse. A similar analysis shows that the internal gravity waves also involve predominantly transverse motions.

For the torsional oscillation modes, a similar local approximation can be developed by applying the condition (29) to equation (23). This yields a result similar to equation (32) for the spheroidal s-modes. For a neutron star with a thin crust, Hansen and Cioffi (1980) have shown that the fundamental ($n = 0$) oscillation mode period is approximately given by

$$\Pi_{t,n=0} \approx \frac{60 \text{ ms}}{[l(l+1)]^{1/2}} R_6 \,. \tag{37}$$

Similarly, the periods of the higher harmonic modes are given by

$$\Pi_{t,n>0} \approx \frac{2 \text{ ms}}{n} \left(\frac{\Delta r}{1 \text{ km}} \right). \tag{38}$$

V. NUMERICAL RESULTS

a) *Mode Spectrum of the Fiducial Model*

The results of our numerical calculations for the spheroidal oscillation modes of the fiducial model are summarized in the mode spectrum shown in Figure 1. This figure displays both the oscillation spectrum of the "three-component" (fluid core plus solid crust plus fluid ocean) fiducial model and, for comparison, the mode spectrum obtained for the same model by treating it as if it were completely fluid ($\mu = 0$ throughout). For the three-component model, we have also included the torsional oscillations in order to provide a complete picture of the oscillation spectra of this star.

As Figure 1 shows, the f- and p-modes are little affected by the presence of the solid crust. This is not surprising since the longitudinal sound speed is generally much higher than the speed of the shear waves ($c_l^2 \gg c_t^2$), so that the speed of an acoustic wave is not greatly affected by the rigidity of the crust. Figure 1 also shows, however, that there are now two types of g-modes: surface g-modes similar to those found in purely fluid models and a new set of g-modes with very long periods (tens of seconds for a model with a central temperature of 10^7 K) that are confined completely to the fluid core. The surface g-modes, which are qualitatively similar to those of the pure fluid model, are largely confined to the ocean, and their periods are somewhat longer than the corresponding modes of the purely fluid model. A new class of spheroidal modes not found in fluid stars is the s-modes. These are shear-dominated modes with periods of about a few milliseconds. Another new class of modes is the interfacial modes (the i-modes). For the fiducial model, the period of the core/crust i-mode is ~ 7 ms, and the period of the ocean/crust mode is ~ 150 ms.

At this point it is appropriate to introduce the nomenclature we use to describe the spheroidal modes. We have opted not to use the geophysical nomenclature, in which all the spheroidal modes are lumped together under the designation ${}_nS_l$ (Lapwood and Usami 1981). Instead, we have endeavored to generalize from the standard astrophysical classification scheme for the p-, f-, and g-modes, first introduced by Cowling (1941), in which the modes are named according to the primary

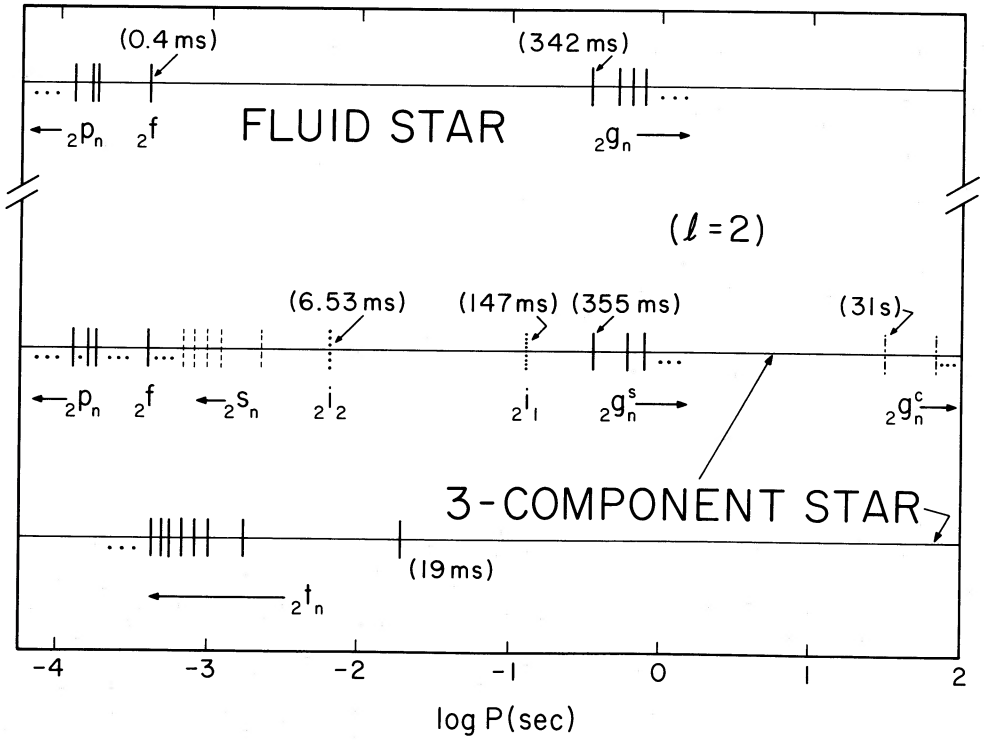

FIG. 1.—The $l = 2$ oscillation spectrum of the "three-component" fiducial model, which contains a fluid core, solid crust, and surface fluid "ocean" (*lower*) and the spectrum of the same model when the shear modulus μ is artificially set to zero throughout ("fluid star", *upper*), both as functions of log period. Lower panel displays both the spheroidal and toroidal modes of the three-component model. See text for a discussion of the spectrum.

TABLE 2

SPHEROIDAL OSCILLATIONS OF FIDUCIAL MODEL

Mode	Period[a]	Period[b]	Period[c]	Energy[a] (ergs)	$(V/U)_{R*}$
${}_2g_2^c$	69.9 s	...	...	2.98+58	...
${}_2g_1^c$	30.9 s	...	...	5.66+57	...
⋮					
${}_2g_3^s$	841 ms	639 ms	692 ms	7.08+43	5.59+6
${}_2g_2^s$	622 ms	521 ms	565 ms	1.23+43	1.13+6
${}_2g_1^s$	355 ms	342 ms	371 ms	1.78+42	2.44+5
${}_2i_1$	147 ms	...	...	2.56+43	3.64+4
${}_2i_2$	6.53 ms	...	...	2.64+52	7.07+1
${}_2s_1$	2.26 ms	...	...	3.14+51	8.49+0
⋮					
${}_2s_9$	0.423 ms	...	...	5.70+50	2.97−1
${}_2f$	0.397937 ms	0.398108 ms	0.412 ms	9.79+50	2.63−1
${}_2s_{10}$	0.384 ms	...	...	5.06+50	2.44−1
⋮					
${}_2s_{19}$	0.195 ms	...	...	1.09+51	6.31−2
${}_2p_1$	0.186 ms	0.189 ms	0.190 ms	1.84+48	5.73−2
⋮					
${}_2p_2$	0.159 ms	0.170 ms	0.171 ms	2.07+47	4.17−2
${}_2p_3$	0.124 ms	0.122 ms	0.124 ms	1.27+47	2.55−2

[a] Computed for three-component model (fluid core, solid crust, fluid ocean).
[b] Periods computed assuming pure fluid, Newtonian pulsation theory.
[c] Periods computed from pure fluid relativistic pulsation theory.

restoring force that is responsible for the oscillations (e.g., gravity, pressure, or shear stress). Hence we have adopted the name *s*-modes for the shear-dominated spheroidal modes.

Following this practice, we designate the *g*-modes by ${}_lg_n^s$ and ${}_lg_n^c$ for the "surface" and "core" modes, respectively. Here l is the spherical harmonic index, and n is the overtone number ($n = 1, 2, \ldots$). The *s*-modes are designated ${}_ls_n$, the single *f*-mode for each l is indicated by ${}_lf$, and the *p*-modes are denoted by ${}_lp_n$. We choose to order the interfacial modes by decreasing period; thus ${}_li_1$ is the interfacial mode with higher period, and ${}_li_2$ is the one with lower period.

The periods and pulsation energies of selected quadrupole modes for the fiducial model are listed in Table 2, where the total time averaged pulsation energy is

$$E = \tfrac{1}{2}\sigma^2 \int_0^{R_*} \rho[U^2 + l(l+1)V^2]r^2 dr\,, \qquad (39)$$

where U and V are defined by equation (9a). Eigenfunctions for some of these modes are displayed in Figures 2–9. Listed in Table 2 are the periods for the three-component fiducial model, the periods derived for the completely fluid fiducial model from a Newtonian analysis, and the periods obtained for the fluid model from relativistic calculations in the Cowling approximation (McDermott, Van Horn, and Scholl 1983). Note that the Newtonian periods given in this and subsequent tables correspond to the local reference frame. The periods observed at infinity can be obtained approximately from these values by applying the appropriate redshift correction: $\Pi_\infty = \Pi_{\rm local}(1-2GM_*/R_*c^2)^{-1/2}$ (see § VIII). Also listed is the time-averaged pulsation energy obtained from the three-component calculations and the ratio V/U of the horizontal amplitude to the vertical (radial) amplitude at the stellar surface. All pulsation energies, except for those of the core *g*-modes, are normalized to unit relative vertical amplitude at the surface. Thus, if the relative radial amplitude at the surface is $(U/r)|_{r=R_*} = 10^{-2}$, then the energies in the table must be multiplied by $(10^{-2})^2$. The core *g*-modes are normalized to unit relative vertical amplitude at the top of the crust. It should be noted that all

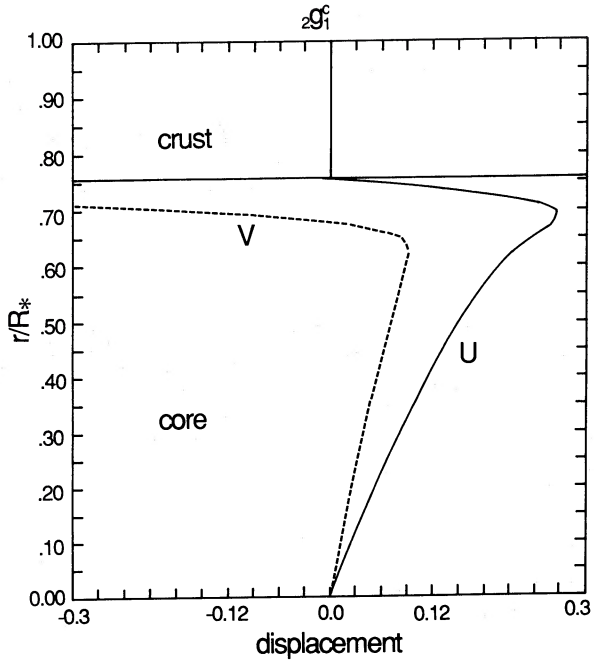

FIG. 2.—The ${}_2g_1^c$ mode displacements vs. fractional radius. The period of this mode is 30.9. The radial displacement U is given by solid curve, and the horizontal displacement V by dashed curve. Note that the motion is almost completely excluded from the solid crust and that the horizontal displacement has a discontinuity at the core/crust interface. The value of V just below the interface is ~ -0.9, and it becomes vanishingly small within the crust.

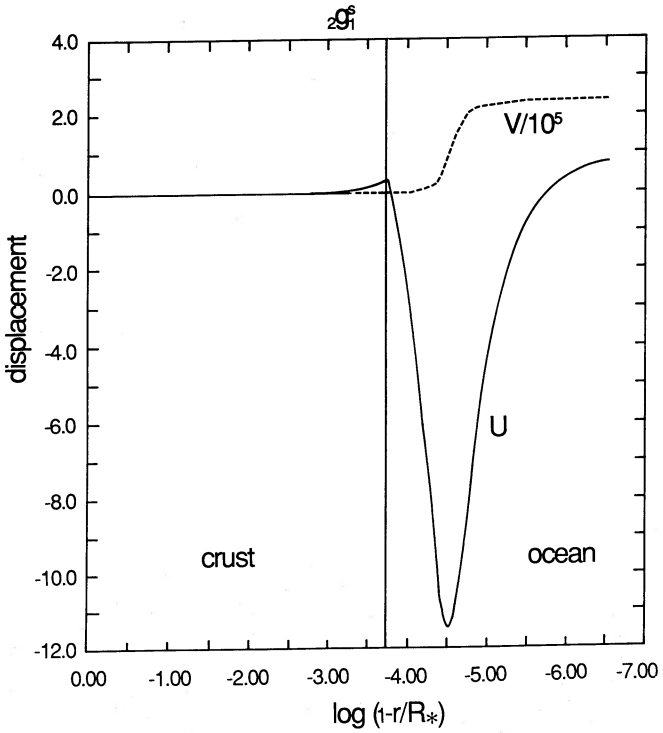

FIG. 3.—The ${}_2g_1^s$ mode displacements. The period is 355 ms. Note the logarithmic abscissa necessary to display this mode. The motion is almost totally confined to the thin fluid ocean [$\log(1 - r/R_*) \leq -3.75$]. The transverse displacement V (*dashed*) has been divided by a factor of 10^5, illustrating the highly transverse nature of these surface *g*-modes.

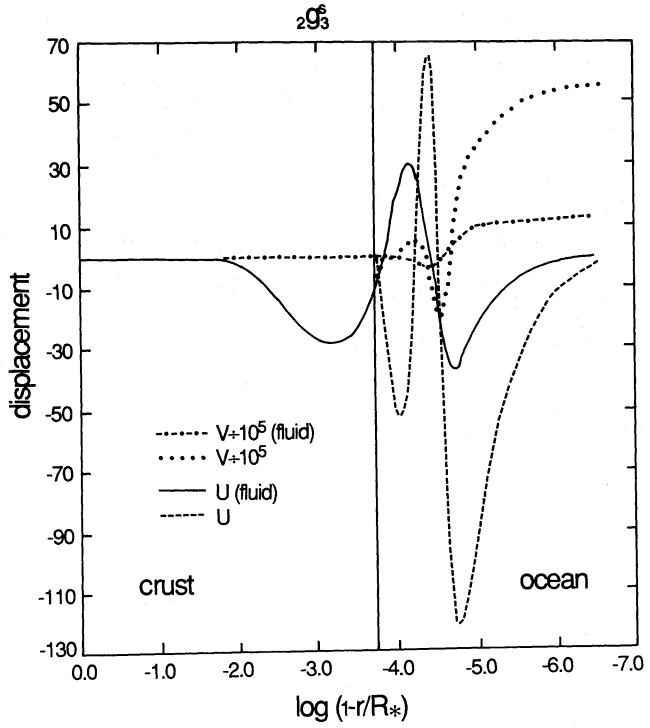

FIG. 4

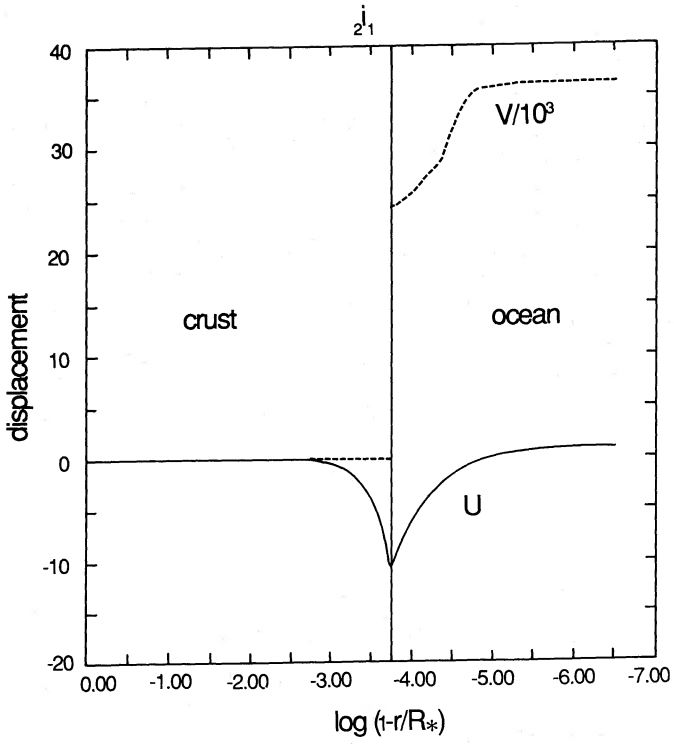

FIG. 5

FIG. 4.—The $_2g_3^s$ mode displacements calculated for the completely fluid fiducial model and for the three-component fiducial model. The effect of the crustal rigidity is to "squeeze" the eigenfunctions out of the crust, resulting in an increase in the period from 639 ms to 841 ms.

FIG. 5.—The $_2i_1$ mode displacements. The period is 147 ms. Note the cusp in the radial displacement U (*solid curve*) at the crust/ocean interface. The transverse displacement V (*dashed curve*), which is divided by 10^3 in this figure, dominates the motion. Note the logarithmic abscissa necessary to display this mode.

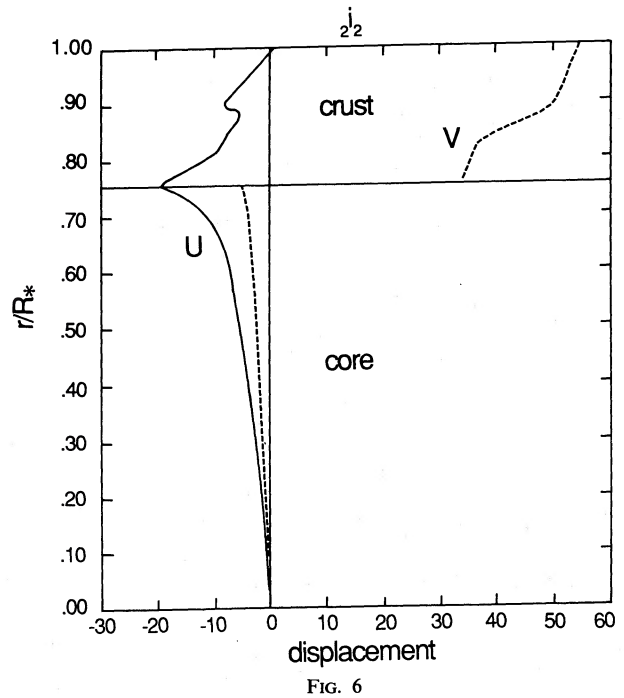

FIG. 6

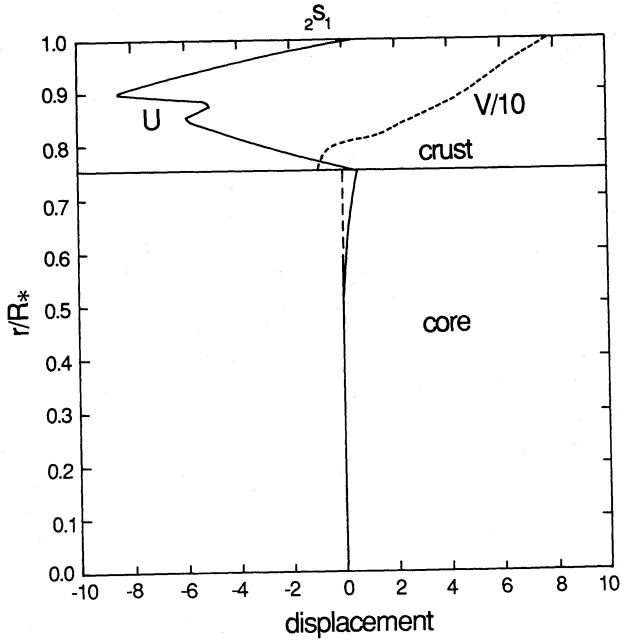

FIG. 7

FIG. 6.—The $_2i_2$ mode displacements vs. fractional radius. The period is 6.53 ms. In this case the $_2i_2$ mode is a core/crust interfacial mode. Note the cusp in U (*solid curve*) at the core/crust interface.

FIG. 7.—The $_2s_1$ mode displacements vs. fractional radius. The period of this mode is 2.62 ms. Note that the eigenfunctions are almost totally confined to the crust and that the transverse displacement (divided by 10, *dashed*) tends to dominate the radial one.

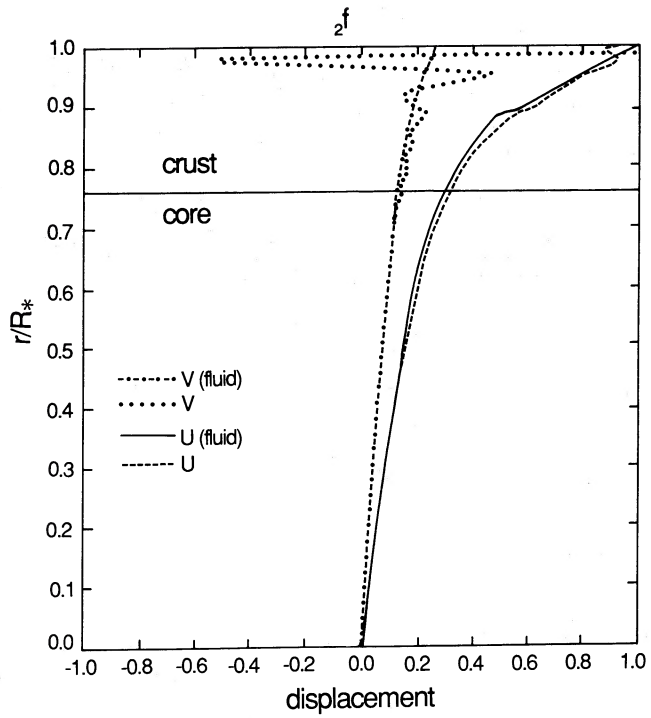

FIG. 8.—The $_2f$ mode displacements calculated for the pure fluid fiducial model and for the three-component fiducial model. Although the period is changed very little by the introduction of the crustal rigidity (see text), the horizontal displacement does exhibit some significant changes.

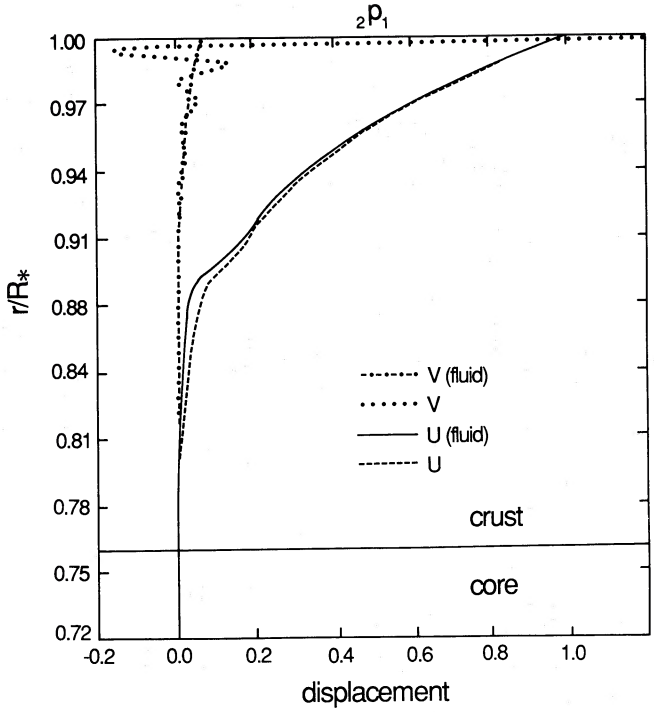

FIG. 9.—The $_2p_1$ mode displacements calculated for the purely fluid fiducial model and for the three-component model. The periods of the p-modes are changed negligibly by the crustal rigidity, but the transverse displacement often exhibits oscillations in the crust, as seen here.

pulsation energies quoted in this paper, unless otherwise noted, are based on unit relative radial amplitude at the stellar surface. This can be misleading, because the radial amplitude is generally orders of magnitude smaller than the transverse amplitude. Some care is therefore necessary in interpreting these energies.

i) *Core g-Modes*

The core g-modes have very long periods, as predicted by equation (36). The reason for this is that the Brunt-Väisälä frequency N, which characterizes the g-modes, is proportional to kT/ϵ_F in degenerate matter, where ϵ_F is the Fermi energy. For conditions near the top of the strongly degenerate, superfluid neutron core, we find $N \sim 0.1$ s^{-1}. These modes are almost entirely confined to the fluid core of the neutron star ($r/R_* < 0.76$), as indicated by Figure 2 for the $_2g_1{}^c$ mode. Note that the horizontal amplitude V has a large discontinuity at the interface. At the boundary of a solid and an inviscid fluid, the fluid can "slip" horizontally past the interface, while the radial displacement U must be continuous.

Even though the amplitudes of these modes are relatively small in the crust, they climb again to large values in the ocean. The behavior of the core g-mode eigenfunctions is not well-determined in the ocean of our model, however, because the mode periods correspond to periods of very high-order surface g-mode overtones. This produces extremely short-wavelength oscillations in the ocean that are not resolved by the zoning in our models. To verify that the basic structure of the core g-modes is being computed correctly, we have therefore carried out many "two-component" calculations, in which it is assumed that the crust extends all the way to the stellar surface. These calculations yield core eigenfunctions which are indistinguishable from those of the "three-component" calculations and periods which are the same to better than six significant digits.

ii) *Surface g-Modes*

The surface g-modes of the fiducial model have periods of 355 ms and longer. The most remarkable features of these modes are the extreme confinement of the displacements to the very outer layers of the neutron star and the overwhelming dominance of the horizontal motion V over the radial motion U. Both of these features are clearly exhibited in Figure 3 for the $_2g_1{}^s$ mode. The effect of the solid crust on the surface g-modes is dramatically illustrated in Figure 4, which shows the $_2g_1{}^s$ fluid mode along with the $_2g_3{}^s$ "three-component" mode. The eigenfunctions are seen to be "squeezed" out of the crust, shortening the effective wavelengths of these modes. This reduction in the effective wavelength causes an increase in the period (see eq. [35]), from 639 ms to 841 ms. The effect of the crust upon the period, at least for the $_2g_3{}^s$ mode, is substantially larger than the relativistic effect (see Table 2).

iii) *Interfacial Modes*

There are two interfacial modes for each value of l in a neutron star with a fluid core, solid crust, and fluid ocean. The identifying characteristic of such modes is a cusp in the radial displacement at the interface. For the fiducial model, the $_li_1$ mode is the crust/ocean interfacial mode, and the $_li_2$ mode is the core/crust interfacial mode. The $_2i_1$ mode has a period of $\sim$147 ms. The displacements are shown in Figure 5. Note that the displacement in the ocean is dominated by the horizontal component. This crust/ocean mode is closely analogous to the Rayleigh waves familiar from geophysics.

The ${}_2i_2$ core/crust mode has a period of ~ 6.5 ms. The displacements are shown in Figure 6. Note the characteristic cusp in U at the core/crust interface. This mode is analogous to the Stoneley mode of geophysics. We have also studied the core/crust interfacial mode in our "two-component" neutron star model and have found periods and eigenfunctions virtually identical to those of the "three-component" calculations. The crust/ocean interfacial mode, of course, is absent for the "two-component" model. In fact, the disappearance of this mode and the surface g-modes provides reassurance that we have correctly identified the association of these oscillations with the crust/ocean interface and with the surface fluid ocean, respectively.

iv) *Shear Modes*

The s-modes have shorter periods than the interfacial modes. For example, the ${}_2s_1$ mode has a period of 2.26 ms. The displacements for this mode are illustrated in Figure 7. The s-modes are almost totally confined to the crust, and the horizontal motion is somewhat larger than the radial motion.

To investigate the properties of the spheroidal shear modes, we have also carried out a number of numerical experiments in which we have artificially reduced the shear modulus μ of the solid crust. As equations (30c) and (32) show, a reduction in μ decreases the shear velocity and increases the periods of the s-modes. Our numerical experiments have confirmed this expectation and provide additional justification for our physical interpretation of these modes.

These reduced μ calculations also have produced dramatic changes in the two interfacial modes, in ways which were not previously anticipated. In particular, as μ decreases, the period of the core/crust mode increases rapidly, and there is interference between this oscillation and the crust/ocean mode. For sufficiently small values of $\mu \lesssim \mu_0/6.5$, where μ_0 is the unreduced shear modulus, these two modes exchange characteristics, exhibiting the phenomenon of "mode bumping" which has been well studied in other contexts (see Pekeris, Alterman, and Jarosch 1962; Aizenman and Smeyers 1977). Continued decrease of μ causes the ${}_2i_2$ mode period to begin to resemble the ${}_2g_1{}^s$ mode of the corresponding purely fluid model (i.e., one with μ set to zero artificially). When the shear modulus is reduced by as much as a factor of 14, the ${}_2i_2$ mode eigenfunction and period are virtually the same as for the fluid ${}_2g_1{}^s$ mode. See McDermott (1985) for a detailed discussion of how the mode spectrum reverts to its fluid form as the shear modulus is reduced.

v) *f-Modes*

The ${}_2f$ mode period, at ~ 0.4 ms, is situated among the higher order s-modes. For the fiducial model the ${}_2f$ mode lies between the ${}_2s_9$ and the ${}_2s_{10}$ modes. The period of the ${}_2f$ mode is changed very little by the introduction of the crustal rigidity; for the fluid fiducial model the period is 0.398108 ms, while for the three-component fiducial model it is 0.397937 ms. The displacements, however, do show some slight changes, as indicated in Figure 8. The elasticity of the crust produces spatial oscillations in the horizontal motion V.

Even though the period of the ${}_2f$ mode is very close to that of the adjacent s-modes, the eigenfunctions are quite distinct. The f-mode has a global character, and the radial displacement is smooth. In contrast, the ${}_2s_{10}$ mode is strongly confined to the outer crust, and the displacements are highly oscillatory.

vi) *p-Modes*

Located among even higher s-mode overtones are the p-modes. Like the f-mode, they are easy to pick out from the midst of the s-modes because their eigenfunctions are clearly distinguishable. The ${}_2p_1$ mode has a period of ~ 0.19 ms, approximately as given by equation (34). The ${}_2p_1$ mode of the three-component model is shown in Figure 9 along with its counterpart for the fluid fiducial model. There is very little difference in the period of the ${}_2p_1$ mode between the fluid and three-component models; indeed we have used this feature to help single out the p-modes in the three-component model. The p-modes are primarily compressional waves, and the speed of a compressional wave is only slightly affected by the shear (see eq. [30c], and note that $\Gamma_1 p \gg \mu$). Note that the p-modes are confined to the outer 10%–20% of the fractional radius and that the radial displacement generally dominates the transverse displacement.

b) Systematic Properties

In addition to the fiducial model, we have constructed three composite neutron star models, as discussed in § III, and have computed the pulsational characteristics of each. Model NS05T7 is the fiducial model with a Gudmundsson envelope; comparison of the results for these two models provides a measure of the sensitivity of different modes to the detailed structure of the neutron star envelope. Model NS05T8 has the same mass as NS05T7, but the central temperature is $T_c \approx 10^8$ K rather than 10^7 K; comparison of the properties of these two models enables us to study the temperature sensitivity of the results. Model NS13T8 has a mass of 1.33 $M_\odot$ and a central temperature similar to that of NS05T8; comparison of these results yields information about the dependence upon the stellar mass. The periods and pulsation energies for each of the composite models are collected in Table 3.

As can be seen by comparing the periods and energies for the fiducial model in Table 2 with those for model NS05T7 in Table 3, the differences in envelope structure produce substantial changes in all but the global p- and f-modes. The qualitative features of the spectrum are the same in both cases, however. The s-modes and the i_2-mode, which "feel" more of the crust, are somewhat more affected than the f- and p-modes. The i_1-mode and the g-modes, which are very sensitive to the properties of the upper crust and the ocean, are of course affected strongly. Surprisingly, the core g-modes also are substantially different. We conjecture that the cause of this is the different phasing of the eigensolution at the core/crust interface that is produced by the different envelope solutions.

Comparison of the results for the different composite models in Table 3 shows that the core and surface g-modes are insensitive to the stellar mass (see eq. [36]) but depend very strongly on the internal temperature, as expected. The core g-mode periods, and to a lesser extent the surface g-mode periods, are approximately proportional inversely to the core temperature. Changes in the core g-mode displacements with mass or temperature, however, are slight; the core g-modes are confined to the core, and the displacements are largest just beneath the interface. In the hotter models, where the ocean is much deeper, the surface g-mode displacements extend much deeper into the star. For these models the ocean is deep enough so that the eigenfunctions appear not to "feel" the crust, at least for low-order modes.

The ${}_2i_1$ and ${}_2i_2$ modes appear to be significantly affected by the internal temperature. In the fiducial model, we have associ-

TABLE 3

PERIODS AND PULSATION ENERGIES OF THE COMPOSITE NEUTRON STAR MODELS

	NS05T7		NS05T8		NS13T8	
MODE	Period	Energy[a] (ergs)	Period	Energy[a] (ergs)	Period	Energy[a] (ergs)
${}_2g_2^c$	88.54 s	2.8+59	8.076 s	1.6+55	7.451 s	3.2+56
${}_2g_1^c$	37.56 s	4.8+58	3.311 s	2.8+54	2.598 s	2.7+55
${}_2g_3^s$	438.9 ms	1.65+40	66.36 ms	6.29+40	61.55 ms	1.96+40
${}_2g_2^s$	368.4 ms	4.39+39	57.41 ms	4.32+41	53.91 ms	1.44+41
${}_2g_1^s$	232.4 ms	4.13+41	49.39 ms	4.93+41	43.67 ms	3.74+41
${}_2i_1$	90.62 ms	8.65+41	13.93 ms	1.43+52	17.72 ms	1.65+53
${}_2i_2$	7.297 ms	3.35+52	7.426 ms	3.84+48	9.911 ms	4.08+47
${}_2s_1$	2.427 ms	2.05+52	2.290 ms	9.10+51	0.7307 ms	1.32+54
${}_2s_2$	1.351 ms	5.73+51	1.294 ms	5.62+51	0.4280 ms	2.53+53
${}_2f$	0.3979 ms	8.33+50	0.3974 ms	1.05+51	0.2299 ms	1.59+52
${}_2p_1$	0.1859 ms	1.96+48	0.1804 ms	1.05+50	0.0831 ms	3.08+51
${}_2p_2$	0.1585	2.18+47	0.1562 ms	1.61+47	0.0598 ms	1.55+50

[a] All energies based on $U(R_*)/R_* = 1$.

ated the ${}_2i_1$ mode with the crust/ocean interface and the ${}_2i_2$ mode with the core/crust interface. This distinction becomes blurred in the hotter models. In the NS05T8 model there is a mode (Fig. 10) that exhibits cusps in the radial displacement at both interfaces. Since identification is problematic, we choose to refer to the higher period interfacial mode as the ${}_2i_1$ and the lower period mode as ${}_2i_2$.

The s-mode periods are relatively insensitive to the temperature but are highly dependent on the mass. The more massive star NS13T8 has much shorter periods s-modes. This is due to the thinner crust and the resulting shorter crossing time for the shear wave. The basic features of the displacements for these modes, however, are unaffected by increments in either mass or temperature. The motion is largely restricted to the crust, and the horizontal motion slightly dominates the vertical displacement.

The ${}_2f$ mode, like the p-modes discussed below, is almost totally insensitive to the internal temperature but does depend on mass. The horizontal displacement shows spatial oscillations in the crust due to horizontal traction, which is absent in the pure fluid models.

The p-modes also are insensitive to internal temperatures. This is because the p-modes are primarily compressional oscillations, and the matter is so highly degenerate that the longitudinal sound speed does not depend on temperature. The p-mode periods scale with mean density fairly accurately as predicted by equation (34). The ratio of the ${}_2p_1$ period in the NS05T8 model to that in the NS13T8 model is 2.17, and in comparison, $(\bar{\rho}[\text{NS13T8}]/\bar{\rho}[\text{NS05T8}])^{1/2} = 2.26$. The p-modes tend to be confined to the outer 20%–30% in fractional radius, and they sometimes show oscillations in the horizontal displacements due to the additional restoring force provided by the crust.

In addition to quadrupole modes, we have also computed $l = 1$, 3, and 4 modes. To compute dipole ($l = 1$) modes it is necessary to rescale the Dziembowski variables (eq. [16]) to avoid singular behavior at $r = 0$ (see McDermott 1985). The resulting pulsation equations then are slightly different in form, but the method of solution is the same, and we have shown by explicit checks at other values of l that our results do not depend on the form of the equations we use. The general l-dependence of the periods is summarized in Figure 11. The fundamental torsional mode ${}_lt_0$ is also displayed to indicate the place of the torsional oscillations in the overall mode spectrum. Generally, the mode periods remain roughly constant or decrease with increasing l. For example, the dependence of the periods of the g-modes on l is predicted quite accurately by the local dispersion relation (33), which gives

$$\Pi_{l+1}/\Pi_l \propto \sqrt{l/(l+2)}\,. \tag{40}$$

The exception to this is the ${}_ls_1$ mode, which increases slightly in period as l is increased.

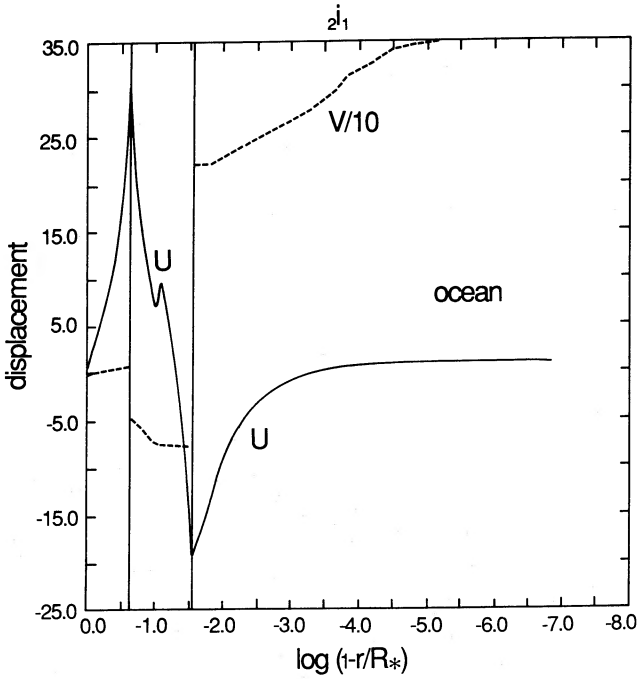

FIG. 10.—The ${}_2i_1$ mode for the NS05T8 model has a period of 13.9 ms. In this interfacial mode, the displacements are confined to *neither* interface. Instead, the radial displacement (*solid curve*) shows cusps at *both* interfaces.

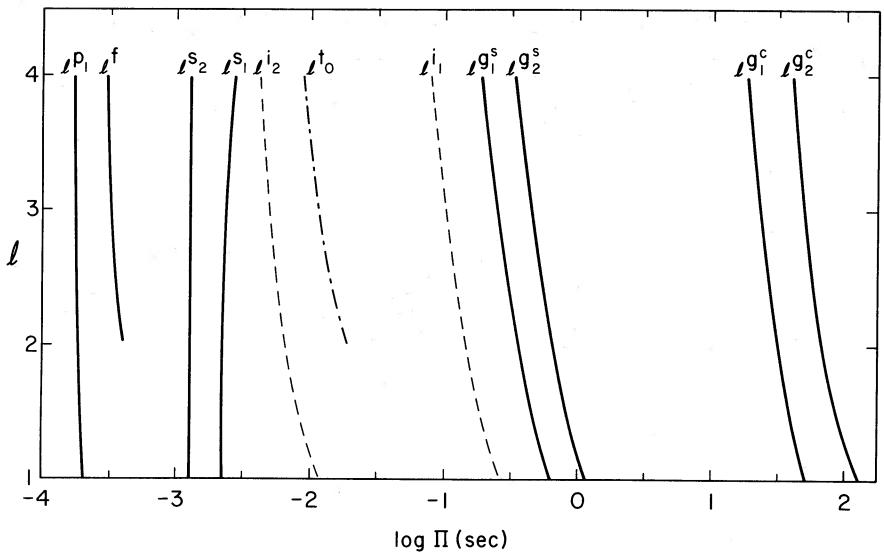

FIG. 11.—Dependence of the mode spectrum of the fiducial model on spherical harmonic index l. At least one of each major subclass of the spheroidal modes is shown. Also displayed is the ${}_{l}t_0$ mode. Note that ${}_{l}f$ and ${}_{l}t_0$ modes do not exist for $l = 1$. Of course, l may only assume integer values.

VI. NUMERICAL RESULTS: TOROIDAL MODES

The spectrum of toroidal modes for the fiducial model is shown, together with the more complicated spheroidal mode spectra, in Figure 1. These modes are essentially the orthogonal polarization of the spheroidal shear (*s*-) modes. The restoring force for the particular subclass of toroidal modes we have investigated, the torsional oscillations, is the finite shear strength of the crust, just as for the *s*-modes. We have therefore named these oscillations *t*-modes, and we use the same convention to distinguish between the different modes. Thus, the ${}_{l}t_n$ mode belongs to spherical harmonic index l and has n nodes in the radial eigenfunction.

This notation is rather different from the geophysical notation for similar modes: ${}_{n}T_{l}$. We use the lower case t and have interchanged the indices n and l relative to the geophysical convention for consistency with conventional usage in stellar pulsation theory. We also note that other classes of toroidal modes are possible in stars with magnetic fields or rotation. Papaloizou and Pringle (1978) have termed the latter *r*-modes, and Carroll *et al.* (1986) have named the former *a*-modes.

The variation of the ${}_{l}t_0$ mode period with l is illustrated in Figure 11, together with the periods of the spheroidal modes. Note that there is no ${}_{l}t_0$ mode. A nodeless dipole mode is incompatible with conservation of angular momentum because dipole modes correspond to oscillatory rotations of the crust.

The mode periods and pulsation energies are listed in Table 4 for the fiducial model and the three composite models. The pulsation energies, given by

$$E = \tfrac{1}{2}\sigma^2 l(l+1)\int_{\text{crust}} \rho W^2 r^2\, dr, \tag{41}$$

are the total time-averaged energies normalized to unit relative amplitude at the top of the crust (i.e., $[W(r)/r]_{r=r_c} = 1$, where r_c is the outer crustal radius).

The periods of the overtones are independent of l, and they are approximately proportional to the crust thickness (see eq. [38]), which is sensitive to the mass. As an example, the ratio of the crust thickness of the NS05T8 model to that of the NS13T8 model is ~ 4.9, and in comparison the ratio of the ${}_{2}t_1$ periods for these models is ~ 5.1. The periods and eigenfunctions of the overtones are almost completely insensitive to l. This can be understood mathematically by examining the pulsation equations (25a)–(25b). The only l-dependent term is the coefficient of S_1 in equation (27b): $l(l+1) - 2 - \sigma^2\rho r^2/\mu$. For $l \lesssim 60$ and periods of ~ 1 ms, the σ^2 term is dominant.

TABLE 4

PERIODS AND PULSATION ENERGIES OF THE FIDUCIAL AND COMPOSITE NEUTRON STAR MODELS

	FIDUCIAL MODEL		NS05T7		NS05T8		NS13T8	
MODE	Period (ms)	Energy (ergs)	Period (ms)	Energy (ergs)	Period (ms)	Energy (ergs)	Period (ms)	Energy (ergs)
${}_{1}t_1$	1.749	1.21+48	1.885	2.06+48	1.795	2.98+48	0.3512	1.09+49
${}_{1}t_2$	1.015	7.95+46	1.097	6.34+47	1.050	1.69+48	0.2079	6.40+48
${}_{1}t_3$	0.8315	4.89+45	0.8199	5.77+46	0.7547	2.91+47	0.1457	1.59+48
${}_{1}t_4$	0.6689	6.00+45	0.7027	7.94+46	0.6382	2.34+47	0.1192	2.72+47
${}_{2}t_0$	19.06	1.25+48	18.59	1.60+48	18.54	1.60+48	17.32	3.31+47
${}_{2}t_1$	1.742	3.67+48	1.877	6.26+48	1.788	9.06+48	0.3512	3.26+49
${}_{2}t_2$	1.014	2.39+47	1.096	1.92+48	1.049	5.13+48	0.2079	1.92+49
${}_{2}t_3$	0.8307	1.46+46	0.8190	1.73+47	0.7539	8.77+47	0.1457	4.76+48
${}_{2}t_4$	0.6685	1.80+46	0.7022	2.38+47	0.6378	7.02+47	0.1192	8.15+47

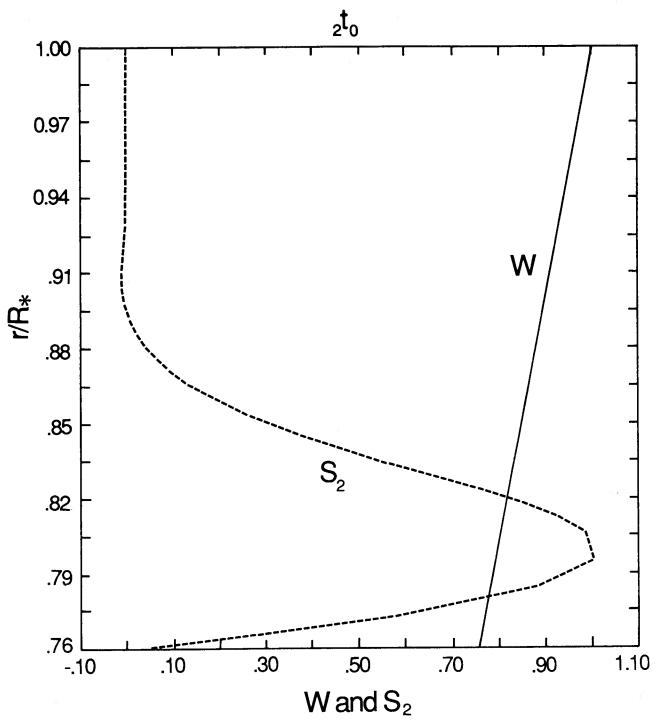

FIG. 12.—The $_2t_0$ eigenfunctions for the NS05T7 model. This mode has a period of 18.6 ms. The transverse displacement $W(r)$ is basically linear in r. The horizontal traction S_2 is shown as a dashed curve.

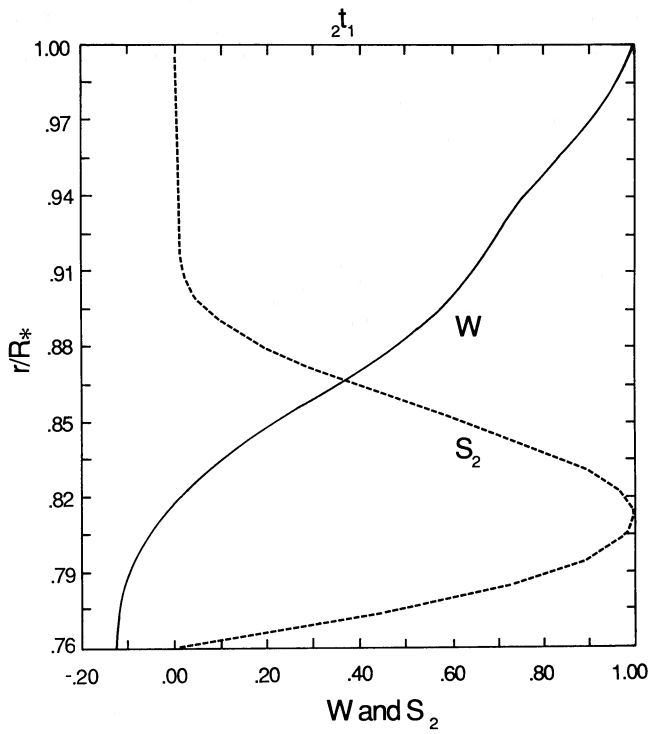

FIG. 13.—The $_2t_1$ eigenfunctions for the NS05T7 model. This mode has a period of 1.88 ms. The transverse displacement is W (*solid*), and the transverse traction is S_2 (*dashed*).

The $_2t_0$ and $_2t_1$ mode eigenfunctions for the NS05T7 model are shown in Figures 12 and 13. We have displayed only the $l = 2$ modes because the eigenfunctions for other l-pole modes are essentially identical (at least for $l \leq 4$). Similarly, eigenfunctions for other models do not differ significantly from those of the NS05T7 model.

Note that the $_it_0$ mode has the character of an interfacial mode; its amplitude is largest at the outer surface of the crust, and the mode period behaves quite differently with changes in parameters than do the other t-modes. It has been demonstrated by Hansen and Cioffi (1980) that the $_it_0$ mode (at least for low l) is almost independent of the stellar mass; our calculations confirm this result. The period of the $_2t_0$ mode is invariably ~ 20 ms. The eigenfunctions of the $_it_0$ modes are almost completely independent of l (at least for small l). The displacement is of a very simple character; to a good approximation $W(r) \propto r$ (see Fig. 12).

We also note that the torsional oscillations are insensitive to the temperature. This result is not surprising because the shear modulus itself is almost independent of the temperature.

VII. DAMPING MECHANISMS

Among the dissipative mechanisms we have investigated are gravitational radiation, neutrino emission, and electromagnetic radiation from an oscillating dipole magnetic field. In schematic form we have also considered nonadiabatic effects and internal friction/viscosity. In the following sections we summarize our calculations for these damping mechanisms for both the spheroidal and the toroidal modes. Our numerical results for the damping times of the different spheroidal modes are given in Table 5 and for the toroidal modes in Table 6.

a) Spheroidal Modes

i) *Gravitational Radiation Damping*

Historically, one of the first damping mechanisms considered for neutron star oscillations was the emission of gravitational radiation. The first completely self-consistent numerical calculations were carried out by Thorne (1969) for quadrupole f- and low-order p-modes. The damping times resulting from these calculations were typically of the order of 1 s. Much more recently, a comprehensive set of quadrupole f-mode calculations has been carried out for 13 equations of state by Lindblom and Detweiler (1983). The damping times quoted by these authors, of the order of tenths of seconds, are claimed to be more accurate than those given by Thorne.

The three-component calculations reported in this paper are based on Newtonian pulsation theory, with the additional assumption that perturbations to the gravitational potential can be neglected (Cowling approximation). These approximations prevent us from performing self-consistent calculations of gravitational radiation damping. We have, however, carried out *a posteriori* estimates of the power radiated and of the consequent damping using the general expression, for $l > 2$, given by Balbinski and Schutz (1982) for the amplitude e-folding time due to the emission of gravitational radiation. In our notation their result is

$$\tau_g = \frac{2E}{L_{\rm GW}} = \frac{\sigma}{2\pi G}\left(\frac{c}{\sigma}\right)^{2l+1} \frac{(l-1)[(2l+1)!!]^2}{l(l+1)(l+2)} \times \frac{\int_0^{R*} dr\rho r^2[U^2 + l(l+1)V^2]}{\{\int_0^{R*} dr\rho r^{l+1}[U + (l+1)V]\}^2}, \quad (42)$$

where $n!! = n(n-2)(n-4)\ldots 1$.

TABLE 5

SPHERICAL MODE DAMPING TIMES

MODE	NS05T7				NS05T8				NS13T8			
	Period	τ_g	τ_v	τ_{em}[a]	Period	τ_g	τ_v	τ_{em}[a]	Period	τ_g	τ_v	τ_{em}[a]
${}_2g_2{}^c$	88.54 s	5.4+15 yr	2.9+3 yr	7.8+31 yr	8.076 s	5.7+13 yr	2.2+2 yr	...	7.451 s	4.5+9 yr	32 d	...
${}_2g_1{}^c$	37.56 s	4.5+13 yr	9.9+3 yr	5.1+52 yr	3.311 s	2.8+10 yr	8.3 yr	...	2.598 s	3.9+7 yr	100 d	...
${}_2g_3{}^s$	438.9 ms	1.4+21 yr	2.3+11 yr	3.4 ms	66.36 ms	3.1+7 yr	7.5 yr	14 ms	61.55 ms	3.7+9 yr	78 yr	0.60 ms
${}_2g_2{}^s$	368.4 ms	2.2+21 yr	7.6+11 yr	9.6 ms	57.41 ms	2.9+7 yr	11 yr	97 ms	53.91 ms	2.4+9 yr	1.3+2 yr	4.6 ms
${}_2g_1{}^s$	232.4 ms	1.6+19 yr	2.8+11 yr	99 ms	49.39 ms	3.0+7 yr	1.8+2 yr	120 ms	43.67 ms	9.3+9 yr	2.2+3 yr	1.3 ms
${}_2i_1$	90.62 ms	1.3+15 yr	3.1+11 yr	0.22 s	13.93 ms	250 d	4.3+2 yr	1.1+2 yr	17.72 ms	10 d	6.6+3 yr	1.7+2 yr
${}_2i_2$	7.297 ms	190 d	4.9+11 yr	2.7+2 yr	7.426 ms	23 yr	4.6+2 yr	11 d	9.911 ms	1.6+2 yr	9.0+2 yr	4.1 hr
${}_2s_1$	2.427 ms	38 d	4.5+14 yr	1.7+2 yr	2.290 ms	140 d	2.2+4 yr	76 yr	0.7307 ms	12 hr	2.5+6 yr	1.6+3 yr
${}_2s_2$	1.351 ms	7.0 d	3.4+16 yr	51 yr	1.294 ms	13 d	1.8+5 yr	51 yr	0.4280 ms	2.8 hr	1.4+8 yr	3.6+2 yr
${}_2f$	0.3980 ms	0.14 s	2.2+14 yr	40 yr	0.3974 ms	0.14 s	2.0+6 yr	48 yr	0.2299 ms	7.5 ms	1.4+8 yr	42 yr
${}_2p_1$	0.1859 ms	0.16 s	7.0+13 yr	1.9 d	0.1804 ms	14 s	4.6+6 yr	91 d	0.0831 ms	0.38 ms	6.9+6 yr	1.4 yr
${}_2p_2$	0.1585 ms	0.24 s	6.7+13 yr	2.1 hr	0.1562 ms	0.29 s	4.5+4 yr	1.5 hr	0.0598 ms	0.23 ms	5.6+6 yr	3.9 d

[a] Assumes $B_0 = 10^{12}$ G and $m = 0$.

TABLE 6

TOROIDAL MODE DAMPING TIMES

MODE	FIDUCIAL MODEL			NS05T7			NS05T8			NS13T8		
	Period (ms)	τ_g	τ_{em}[a]	Period (ms)	τ_g	τ_{em}[a]	Period (ms)	τ_g	τ_{em}[a]	Period (ms)	τ_g	τ_{em}[a]
${}_1t_1$	1.749	...	220 d	1.885	...	1.58 yr	1.795	...	1.9 yr	0.3512	...	14 d
${}_1t_2$	1.015	...	1.6 d	1.097	...	20 d	1.050	...	47 d	0.2079	...	1.0 d
${}_1t_3$	0.8315	...	1.1 hr	0.8199	...	14 hr	0.7547	...	2.2 d	0.1457	...	1.5 hr
${}_1t_4$	0.6689	...	34 m	0.7027	...	10 hr	0.6382	...	21 hr	0.1192	...	6.8 m
${}_2t_0$	19.06	7.3 + 3 yr	3.0 + 7 yr	18.59	5.2 + 3 yr	3.3 + 7 yr	18.54	5.2 + 3 yr	4.0 + 7 yr	17.32	2.1 + 4 yr	3.2 + 7 yr
${}_2t_1$	1.742	3.3 yr	51 yr	1.877	3.7 yr	1.6 + 2 yr	1.788	2.9 yr	1.8 + 2 yr	0.3512	8.8 d	80 d
${}_2t_2$	1.014	2.7 yr	47 d	1.096	2.1 yr	2.0 yr	1.049	1.8 yr	4.2 yr	0.2079	2.7 d	2.0 d
${}_2t_3$	0.8307	1.9 yr	21 hr	0.8190	250 d	11 d	0.7539	150 d	37 d	0.1457	4.2 hr	1.4 hr
${}_2t_4$	0.6685	100 d	7 hr	0.7022	112 d	6.2 d	0.6378	99 d	11 d	0.1192	1.3 hr	9.4 m

[a] Assumes $B_0 = 10^{12}$ G. For $l = 1$, $|m| = 1$. For $l \geq 2$, $m = 0$.

Calculations based on equation (42) show that gravitational radiation is a very efficient damping mechanism for the f- and p-modes. For the 0.5 $M_\odot$ models, the damping times are a few tenths of seconds, in basic agreement with the results of Lindblom and Detweiler (1983). The 1.3 $M_\odot$ model, however, has much shorter decay time scales. The ${}_2f$ mode of this model has a damping time of ~ 10 ms, and the low-order (in n) p-mode damping times are tenths of milliseconds. Higher order l-pole modes are somewhat longer lived. For example, the ${}_3f$ and ${}_3p_1$ modes of the fiducial model have damping times $\tau_g \sim 10$ s. Because of the short lifetimes of the f- and p-modes, however, it is unlikely that they will be observed, except perhaps as transient phenomena.

In constrast to the p-modes, the core g-modes are very inefficiently damped by gravitational radiation, despite the fact that these modes are confined to the core and therefore involve bulk motions of large amounts of mass. The reason is that $\tau_g \propto \sigma^{-4}$ (for $l = 2$), and the frequencies of the core g-modes are very low. Typical quadrupole dissipation times range from 10^7 yr for NS13T8 up to 10^{15} yr for the NS05T7 model.

The surface g-modes also are very weakly damped by gravitational radiation because the frequencies of these modes, too, are relatively low. In addition, the displacements in the surface g-modes involve very small amounts of mass. Typical quadrupole damping times range from 10^7 yr (NS05T8) up to 10^{21} yr (NS05T7). Higher order l-pole modes have even longer dissipation times.

The low order (in n) ${}_2s_n$ modes, which are intermediate in both period and mass motions between the p- and g-modes, have intermediate gravitational radiation damping times covering a broad range from 10^4–10^7 s.

ii) *Neutrino Damping*

The early cooling of neutron stars is overwhelmingly dominated by neutrino emission. Because neutrino cooling is so important, it is necessary to ask whether oscillations may be significantly damped by pulsed neutrino emission. Previous calculations of neutrino damping of neutron star oscillations generally fall into two categories (see Sawyer 1980, and references therein). In the first, oscillations are damped by the net excess of emission averaged over a pulsation cycle. In the second category, the emission of neutrinos derives from pulsation-induced departures from β-equilibrium. As the density changes during the pulsation, the relative concentrations of neutrons, protons, and electrons changes, causing a departure from chemical equilibrium.

We have evaluated the neutrino damping of neutron star oscillation modes using a quasi-adiabatic analysis. This technique is discussed in general by Cox (1980) and in particular for neutrino damping of white dwarf pulsations by Osaki and Hansen (1973). The damping time is given by

$$\tau_\nu \approx \frac{4E}{C}, \tag{43}$$

where $C = \int (\delta T/T)^* \delta\epsilon_\nu \, dM_r$, and E is the time-averaged pulsation energy (eq. [39]). The Lagrangian perturbations to the neutrino emissivity can be expressed in terms of the temperature and density perturbations as follows:

$$\delta\epsilon_\nu = \frac{\partial\epsilon_\nu}{\partial \ln T}\bigg|_\rho \frac{\delta T}{T} + \frac{\partial\epsilon_\nu}{\partial \ln \rho}\bigg|_T \frac{\delta\rho}{\rho}, \tag{44}$$

where

$$\left(\frac{\delta T}{T}\right)_{\rm ad} = \Gamma_1 \nabla_{\rm ad} \frac{\delta\rho}{\rho}. \tag{45}$$

Note that the quasi-adiabatic analysis implicitly assumes that the matter remains in chemical equilibrium throughout the pulsation cycle. This may not be valid if the relaxation times of the principal neutrino-producing reactions are long in comparison to the pulsation period, and future studies should investigate the validity of this assumption.

Neutrino damping is most effective for the core g-modes of the hotter models. For example, in the NS13T8 model, the ${}_2g_2{}^c$ mode has a damping time of $\tau_\nu \sim 9 \times 10^{-2}$ yr. In the cooler (NS05T7) model, with much lower neutrino emission, the core g-mode damping times are $\tau_\nu \sim 10^3$–10^4 yr. These results for the core g-modes are critically dependent on the presence of the pion condensate assumed by Richardson (1980). The emissivity due to "quasi-particle β-decay" (see Richardson *et al.* 1982) in the pion condensate is proportional to T^6, and for this reason, core mode pulsations of the cooler models are much less efficiently damped than they are for the hotter models.

The surface g-modes are only weakly damped by neutrino emission. For the hotter models, typical damping times are 10–1000 yr. The cooler model is exceedingly weakly damped, with $\tau_\nu \sim 10^{11}$ yr. The emission process responsible for damping in the hotter models is a combination of the plasma process and crust bremsstrahlung.

For the interfacial modes, the neutrino damping times are generally longer than the gravitational radiation damping times, sometimes by several orders of magnitude. For the shorter period s-, f-, and p-modes, the neutrino damping is insignificant in comparison to gravitational radiation losses. The reason for the inefficiency of neutrino damping in these cases is that the pulsation energies of the s-, f-, and p-modes are much larger than those of the surface g-modes, while the neutrino processes that are most effective are essentially the same as for the surface g-modes. The f- and p-mode eigenfunctions are not large enough in the region where pion-assisted neutrino emission is important for that process to be an effective damping mechanism for these modes. For the s-modes the eigenfunction actually vanishes in the core. The i-modes must each be considered separately, and the results depend upon whether a particular mode is more "g-like" or "p-like" in character.

iii) *Electromagnetic Damping*

Because the magnetic field decay time in neutron star matter is much longer than the period of any pulsation, the magnetic field is effectively frozen into the matter on the pulsation time scale. During pulsations the field oscillates with the matter, and this produces electromagnetic radiation, which can drain energy from the oscillation.

We have made an *a posteriori* estimate of the power radiated by a magnetic dipole field frozen into a pulsating neutron star, under the assumption that the field does not significantly alter the pulsation periods or displacements. The details of this calculation and further discussion of the approximations and assumptions have been reported elsewhere (McDermott *et al.* 1984*b*). The estimated damping times are listed in Tables 5 and 6. Note that $\tau_{\rm em} \propto {B_0}^{-2}$ and that the tables are based on $B_0 = 10^{12}$ G. Recent work by Carroll *et al.* (1986) includes the effects of the field on the oscillations self-consistently for a simplified, cylindrical model of the polar regions of a neutron star. These

calculations have shown that for sufficiently large values of B_0 the field dramatically alters the character of the surface g-modes, which are primarily concentrated in the outermost layers of the neutron star. The field essentially leaves the other modes of the star unaffected, however. These calculations also show that the estimates of electromagnetic damping times which are given in Table 5 are too long, in some cases by as much as a factor of 100.

We have estimated the electromagnetic damping times for all of the spheroidal modes, although the results for the surface g-modes and the crust/ocean interfacial mode have no meaning for $B_0 = 10^{12}$ G, since these modes are radically altered by such fields. For $l \geq 2$, all modes shorter in period than the ${}_lg_n^s$ modes are damped more efficiently by gravitational radiation than by electromagnetic damping.

For the dipole modes, there is no gravitational radiation, and the electromagnetic power radiated is

$$P(l = 1, m = 0) = 2 \times 10^{43}\left(\frac{2V + U}{R_*}\right)^2\left(\frac{B_0}{10^{12}/\mathrm{G}}\right)^2 \times \left(\frac{R_*}{10^6\ \mathrm{cm}}\right)^8\left(\frac{0.2\ \mathrm{ms}}{\Pi}\right)^6\ \mathrm{erg\ s^{-1}}, \quad (46)$$

where U and V are the radial and transverse displacements evaluated at the surface of the neutron star. For the f- and p-modes, a typical pulsation energy is $\sim 10^{50}(U/R_*)^2$ ergs, which leads to a damping time of $\tau_{\mathrm{em}} \sim 0.1$ yr. For all other dipole modes, the longer periods yield damping times $\tau_{\mathrm{em}} \sim 10^8$ yr, much too long to be of interest. Ohmic dissipation effects due to small relative motions of the matter with respect to the field lines have been shown to be generally insignificant (Carroll *et al.* 1986).

iv) *Nonadiabatic Effects*

The motion of perturbed matter elements during a pulsation is nearly, but not precisely, adiabatic. The slight departures from adiabaticity, however, can dissipate energy from the pulsations. For example, heat flow down the temperature gradients associated with the pulsation is such a dissipative mechanism. Carroll (1982, private communication) has carried out a quasi-adiabatic analysis of this effect for the surface g-modes of the pure fluid fiducial model (assumes $\mu \equiv 0$; see § III). He finds that the surface g-modes are efficiently damped by this mechanism. For the ${}_2g_1^s$ mode (371 ms period) the decay time he obtains is ~ 100 s, and the overtones generally have shorter damping times.

These results are rather uncertain, however, because the surface layers of the fiducial model are only crude, polytropic approximations and because they do not allow for partial ionization of ^{56}Fe. Thus, the opacity and its temperature and density derivatives, which are needed accurately as input to the quasi-adiabatic calculations, are only crudely represented. In addition, the large discontinuity in luminosity between the envelope and interior in the composite models renders thermal damping calculations suspect for those cases as well. Further study is obviously warranted.

b) Toroidal Modes

i) *Gravitational Radiation Damping*

For the torsional oscillations, there is no net mass l-pole moment because $\delta\rho$ and u_r are identically zero for these modes. As a consequence, there is no mass quadrupole or higher order mass l-pole gravitational radiation from the torsional oscillations. Instead, the gravitational radiation must come from "mass currents." Schumaker and Thorne (1983) have provided a prescription for computing the damping time for such cases in the weak field, slow motion limit. In our notation, the amplitude damping time is

$$\tau_g = \left(\frac{c}{8\pi G}\right)\left(\frac{c}{\sigma}\right)^{2l+1}\frac{(l-1)[(2l+1)!!]^2\int_{\mathrm{crust}}\rho r^2 W^2\,dr}{(l+2)(\int_{\mathrm{crust}} r^{l+2}\rho W\,dr)^2}. \quad (47)$$

Schumaker and Thorne estimate that the damping time of a fundamental quadrupole torsional oscillation is $\tau_g \sim 10^4$ yr.

Gravitational radiation is an inefficient damping mechanism for the torsional oscillations. We find the damping times of the ${}_2t_0$ modes to be $\sim 10^3$–10^4 yr, in agreement with the estimate of Schumaker and Thorne (1983), although the overtones are damped much more rapidly. For the 0.5 $M_\odot$ models, the damping times are typically $\lesssim 1$ yr for the first few quadrupole overtones. The 1.3 $M_\odot$ model, however has much shorter overtone periods, and as a result these modes decay much more quickly. The ${}_2t_n$ modes for this model have dissipation times ranging from $\sim 10^{-2}$ yr (for $n = 1$) to $\sim 10^{-4}$ yr (for $n = 4$).

For higher l-pole modes, gravitational radiation is much less effective, and the damping times rise rapidly. As an example, for the NS05T7 model the ${}_3t_0$ mode has a damping time of $\sim 10^8$ yr, and the ${}_4t_0$ mode decay time is $\sim 10^{12}$ yr.

ii) *Nonadiabatic Effects and Neutrino Losses*

For the torsional oscillations, the quasi-adiabatic analysis fails to provide a nonzero damping rate for the neutrino damping. Recall that one of the properties of the torsional oscillations is that $\delta\rho \equiv 0$. This in turn implies that $(\delta T)_{\mathrm{ad}} = 0$ (see eq. [45]), so that there is no damping due to nonadiabatic effects. With $\delta\rho$ and δT both zero, there is also no dissipation of pulsation energy due to modulated neutrino emission (see eq. [44]). Since we believe that the adiabatic eigenfunctions are good approximations to the nonadiabatic eigenfunctions, it seems likely that even in a fully nonadiabatic calculation the damping of the torsional oscillations via nonadiabatic effects and neutrino emission will be very weak.

iii) *Electromagnetic Damping*

The electromagnetic damping time for the dipole modes is 1 yr, depending upon the period. For the quadrupole modes, the ${}_2t_0$ damping time is $\tau_{\mathrm{em}} \sim 10^7$ yr, much longer than the gravitational radiation damping time. For the overtone ${}_2t_n$ modes, however, electromagnetic damping becomes increasingly important. As an example, for the ${}_2t_3$ mode in the NS05T7 model, $\tau_{\mathrm{em}} \sim 0.03$ yr, whereas $\tau_g \sim 0.7$ yr. Note, however, that for successively higher overtones, the slow motion approximation (see Schumaker and Thorne 1983) becomes less satisfactory, and therefore both τ_g and τ_{em} become less reliable.

iv) *Internal Friction and Viscosity*

In terrestrial solids, sound waves are damped by internal friction. It is conceivable that internal friction may be the principal dissipative mechanism for some of the neutron star oscillation modes, particularly those for which other damping mechanisms are weak (e.g., torsional oscillations). The crustal lattice is likely to be filled with various defects and impurities which enhance this dissipation. In cooled, single crystal laboratory samples of silicon or sapphire, Q-values of up to $\sim 10^9$ have been achieved (see Douglass and Braginski 1979), where $Q \equiv \pi\tau/\Pi$. A $Q \lesssim 10^9$ for neutron star matter would lead to a damping time $\tau \lesssim 0.1$ yr for the torsional oscillations.

Landau and Lifshitz (1970) have shown that the formalism for handling internal friction is completely analogous to that for the viscosity of a fluid. They introduce a dissipative stress tensor which, for the torsional oscillations where $u_{ll} = 0$, reduces to $\delta\tau_{ik} = 2\eta\dot{u}_{ik}$, where η is the shear "viscosity." The damping time of the torsional modes is expected to be roughly $\tau \sim (2\rho r^2/\eta)$, where ρ and η are to be evaluated near the peak of the displacement, $W(r)$. For the ${}_2t_0$ mode this peak occurs near nuclear density, $\rho \sim 10^{14}$ g cm^{-3}.

It is an understatement to say that the determination of the internal dissipation in neutron star matter is fraught with difficulties and uncertainties. Even in terrestrial matter there are many damping mechanisms that cannot be accounted for by known processes (Johnson 1982, private communication). Flowers and Itoh (1976) have nevertheless made estimates of the viscosity of neutron star matter, principally for temperatures below the melting point of the crust. However, they have computed only the electronic contribution to the viscosity, including the following scattering processes: electron-phonon, electron-impurity, electron-electron, and electron-neutron, the latter for densities above neutron drip. Examination of Tables 1 and 4 of their paper shows that for $T = 10^8$ K, the electron-phonon contribution dominates all other mechanisms for all densities, even for unreasonably large impurity concentrations ($x_i \sim 1$) and for large values of $(Z_i - Z)^2$, where Z_i is the impurity atomic number, and Z is the atomic number of the equilibrium species. For $T = 10^7$ K the electron-phonon contribution is still dominant unless $x_i(Z_i - Z)^2 \gtrsim 10^{-2}$. If the electron-phonon contribution is in fact dominant, then for $T = 10^8$ K and $\rho \sim 10^{14}$ g cm^{-3}, we obtain $\eta \sim 3 \times 10^{14}$ poise, and for $T = 10^7$ K and $\rho \sim 10^{14}$ g cm^{-3}, we have $\eta \sim 3 \times 10^{16}$ poise. Thus our estimates of the damping times of the torsional oscillations are $\tau \sim 10^4$ yr for 10^8 K models and $\tau \sim 10^2$ yr for 10^7 K models. This gives a Q ranging from 10^{11}–10^{13}, or 10^3–10^5 times higher than that achieved in the terrestrial laboratory. Flowers and Itoh, however, do not treat the ionic contribution to the internal friction or viscosity. This contribution may in fact be dominant, and its neglect probably means that the quoted viscosities are underestimates, perhaps by many orders of magnitude. Thus, the damping time scales associated with these processes are highly uncertain. They are sufficiently small, however, to provoke interest and warrant further investigation. Very recently Cutler and Lindblom (1987) have examined the effect of viscosity on the f-mode. They find a damping time of ~ 1 yr for typical neutron star parameters.

VIII. SUMMARY AND CONCLUSIONS

Even in the absence of rotation and magnetic fields the normal mode spectrum of a neutron star is far more complex and diverse than is generally recognized. We have carried out the present investigation to help illuminate this complexity and to provide a foundation for interpreting the quasiperiodic oscillations seen in some pulsars and X-ray burst sources.

Both the core and surface g-modes of neutron stars have periods which vary inversely with the core temperature. The core g-modes are almost totally confined to the fluid interior of the neutron star and have long periods ($\Pi_g{}^c \gtrsim 3$ s for $T_c \lesssim 10^8$ K). Because of their very large pulsation kinetic energies, $\sim 10^{55}$–10^{58} ergs for unit relative radial amplitude at the base of the crust, these modes are unlikely to be excited to observable amplitudes except perhaps in the supernova core collapse which forms the neutron star. The most efficient damping mechanism we have identified for these modes is neutrino emission, which is most effective in the hotter models ($\tau_\nu \sim$ 0.1–100 yr) and which depends on the presence of an assumed pion condensate. For such rapid damping, any core g-mode oscillations triggered by the formation of a neutron star are unlikely to remain observable following dissipation of the supernova remnant shell. If such pulsations were to be detected, this would provide strong evidence against the existence of a pion condensate in those neutron stars. The periods of the core g-modes are probably only accurate to within $\sim 25\%$ because of our use of the Cowling approximation and because of uncertainties in the location of the core/crust interface. Rotational effects, which we have not treated, also are likely to be important, and the mode properties are likely to be affected strongly by superfluidity of neutrons and protons in the core.

The surface g-modes have periods $\Pi_g{}^s \gtrsim 50$ ms for $T_c \lesssim 10^8$ K. The periods are sensitive to the depth of the surface fluid ocean, and the modes are "squeezed" out into the ocean by the advancing crust as the neutron star cools. With pulsation energies $\lesssim 10^{33}$ ergs for unit relative *transverse* amplitude at the surface, these modes may be excited to observable amplitudes by accretion-fed thermonuclear outbursts (McDermott and Taam 1987) and may thus lead to observable quasiperiodic oscillations in X-ray burst sources. Of the three composite models used in the present pulsation calculations, the NS13T8 model has physical properties most similar to those expected in the envelope of an X-ray burst source. The ${}_2g_1{}^s$ mode period for this model is 44 ms, right in the middle of the 10–70 ms range of the observed periodicities (Livio and Bath 1982). The pulsation displacements are large in the region where the nuclear burning occurs, a condition necessary for efficient excitation by the burning region. Furthermore, the surface g-modes have relatively low pulsation energies, another condition for ease of excitation. The ${}_2g_1{}^s$ mode of the NS13T8 model has an energy $E = 1.1 \times 10^{33}[V(R_*)/R_*]^2$ ergs. Even if only a minute fraction ($\sim 10^{-6}$) of the 10^{39} ergs released in an X-ray burst could be channeled into oscillations, the surface g-modes would be driven to high amplitudes. Rotation periods $\lesssim 0.1$ s are likely to be important for these modes, and typical pulsar magnetic fields will radically alter them.

The effect of general relativity on the periods of the surface g-modes is very accurately predicted by the redshift of the neutron star (Carroll 1982, private communication). Because the surface g-modes are so highly localized in the outer layers, they have the character of a local clock. The period of such a clock, as seen from infinity, is simply computed by applying the redshift correction to the local period. For the fiducial model this gives $\Pi_\infty = \Pi_{\rm local}(1 - 2GM_*/R_*c^2)^{-1/2} = 1.0828\Pi_{\rm local}$, to be compared to our relativistic mode calculations, which result in $\Pi_\infty/\Pi_{\rm local} = 1.083 \pm 0.002$, for low-order quadrupole modes.

The interfacial modes have periods intermediate between those of the surface g-modes and the s-modes. In the fiducial model, the ocean/crust interfacial mode, with period ~ 150 ms and pulsation energy $\sim 10^{43}$ ergs, has the character of a Rayleigh wave. This mode, like the surface g-modes, is potentially capable of being excited in X-ray burst sources. The mode properties, including the period, are extremely sensitive to structural details near the ocean/crust boundary. We do not know the primary damping mechanism for this mode; it may be due to nonadiabatic effects, as appears to be the case for the ${}_1g_n{}^s$ modes. Also like those modes, the properties of this inter-

facial mode appear to be radically altered by strong magnetic fields. The crust/core interfacial mode, with period ~ 6.5 ms and pulsation energy $\sim 10^{52}$ ergs in the fiducial model, has the character of a Stoneley mode. This mode appears to require more energy than is expected to be available in order to be excited in an X-ray burst source. It is damped by gravitational radiation in ~ 200 days.

The *s*-modes are essentially normal modes of spheroidal shear waves, and the displacements are largely confined to the crust. The periods are sensitive to the crust thickness and range between 1–2 ms for the ${}_2s_1$ mode. Pulsation energies are $\sim 10^{52}$ ergs for the 0.5 $M_\odot$ models but are lower for the higher masses. In all cases, the energies are so high that these modes probably cannot be excited to observable amplitudes. Gravitational radiation is moderately effective in damping these modes, with damping times ~ 0.5–100 days. These modes and other short-period modes are likely to be essentially unaffected by magnetic fields or rotation, except perhaps for millisecond rotation periods.

The *f*-mode and the *p*-modes have short periods ($\Pi \lesssim 0.2$ ms for the ${}_2f$ and ${}_2p_1$ modes) and large pulsation energies, $\sim 10^{48}$–10^{51} ergs, mitigating against their potential observability. They are very efficiently damped by gravitational radiation, with damping times ranging between 10 and 100 ms. The *f*-mode has a global character and may be affected by superfluidity. Neglect of the gravitational potential perturbations results in errors of $\lesssim 25\%$ in our estimate of the period. The *p*-modes are restricted to the outer $\sim 20\%$ in fractional radius, and the Cowling approximation therefore has little effect on the periods.

The torsional oscillations are normal modes of toroidal shear waves in the neutron star crust. The ${}_2t_0$ mode period is invariably ~ 20 ms, and the overtone periods are directly proportional to the crust thickness [${}_l\Pi_n \approx (2\Delta r/n)$ ms, where Δr is the crust thickness in kilometers]. These modes have pulsation energies $\sim 10^{48}$–10^{49} ergs. The damping mechanisms we have considered for these modes are all relatively weak. For example, gravitational radiation damping is the dominant energy loss mechanism among the ones we have considered for the ${}_2t_0$ mode, but the damping time is $\tau_g \sim 10^3$–10^4 yr. Depending on the magnetic field strength, the values of l and m, and the temperature of the neutron star, the damping could be dominated by gravitational radiation, with $\tau_g \lesssim 1$ yr, electromagnetic radiation, with $\tau_{\rm em} \lesssim$ days, or possibly internal friction, perhaps with τ_{if} on the order of days to years. Torsional oscillations could be excited in a pulsar macroglitch, although the amplitude seems likely to be small. A pulsar macroglitch is manifested by an abrupt increase in rotational frequency. Observations of the Vela pulsar indicate that $\Delta\Omega/\Omega \sim 2 \times 10^{-6}$ (Taylor and Manchester 1977). The sudden spin-up corresponds to a release of internal energy $E \sim 1/2I\Omega^2(\Delta\Omega/\Omega)$, where I is the moment of inertia of the neutron star. Assuming values of $I \sim MR^2 \sim 10^{45}$ g cm^2 and $\Omega \sim 10$ (for the Vela pulsar), the energy released is $E \sim 10^{41}$ ergs. Conceivably such an event could excite torsional oscillations which might persist long enough to be observable. The energy of a typical torsional oscillation mode is $E \sim 10^{48}[W(R_*)/R_*]^2$ ergs. If all the energy of a glitch were channeled into a single torsional mode, an amplitude of $W(R_*)/R_* \sim 10^{-4}$–10^{-3} could be expected. It is not yet known how large an amplitude is necessary to produce an observable perturbation of the pulsar emission mechanism.

There are many potentially important effects for real neutron stars that we have not included in our analysis of the "three-component" oscillation spectrum but have noted in passing. Among these are superfluidity, rotation, magnetic fields, and general relativity.

Superfluidity of the neutrons in the inner crust, and of the protons and neutrons in the core, may have a significant effect on modes with large core amplitudes, such as the core *g*-modes and the *f*-mode. For example, vortex unpinning may produce substantial damping of these modes. In addition, there may be new modes ("Tkachenko" oscillations; see Ruderman 1970) that arise specifically from the properties of superfluids.

Radio pulsars have typical magnetic field strengths of 10^{12} G. As shown by Carroll *et al.* (1986) and as noted above, the surface modes (${}_lg_n^s$ and the crust/ocean interfacial mode) will be profoundly altered by such large fields. The magnetic pressure is $P_{\rm mag} = B^2/8\pi \sim 4 \times 10^{22} B_{12}{}^2$ dyne cm^{-2}, where $B_{12} \equiv B_0/10^{12}$ G, and if we assume an ideal, degenerate, non-relativistic electron gas for the surface layers, then the gas pressure is $P_{\rm gas} \sim 3 \times 10^{12}\rho^{5/3}$ dyne cm^{-2} (assuming $\mu_e = A/Z = 2$). Thus the magnetic pressure dominates until $\rho \gtrsim 10^6 B_{12}{}^{6/5}$ g cm^{-3}. This implies, for example, that the entire ocean of the NS05T7 model would be dominated by magnetic effects.

Radio pulsars also have a very broad range of observed rotation periods, from 1.6 ms to ~ 4 s. When the period of an oscillation mode is comparable to or longer than the rotation period, rotational effects are expected to be important. Even for the most slowly rotating neutron stars, the core *g*-modes are likely to be strongly affected by the rotation. For millisecond pulsars all the modes, with the possible exception of the *f*- and *p*-modes, are likely to be radically altered by the rapid rotation.

If neutron star oscillations can be observed, then as the calculations reported in this paper show, they are potentially capable of providing important new fundamental information about the interior conditions of these extremely dense objects.

We wish to thank M. B. Richardson for providing us with the equilibrium models and E. H. Gudmundsson for sharing the details of his envelope calculations with us. Special thanks to B. W. Carroll for checking the Cowling approximation and estimating the nonadiabatic damping of the surface *g*-modes. Finally, we express our gratitude to M. P. Savedoff, R. Buland, and G. Masters for helpful suggestions and advice. This work has been supported by the National Science Foundation through grants AST 83-07214 and AST 85-11173 through the University of Rochester, AST 83-15698 and AST 85-15489 through the University of Colorado, and AST 81-09826A01 through Northwestern University. One of us (P. N. McD.) also gratefully acknowledges support through Northwestern University by the Lindheimer Fellowship fund and the NASA Astrophysics Theory Program under grant NAGW-768. One of us (H. M. V. H.) also wishes to thank the Department of Astronomy at the University of Texas (Austin) for their generous hospitality during the final preparation of this manuscript.

APPENDIX

NUMERICAL METHOD

The spheroidal and toroidal eigenvalue problems described by equations (13), (18), (19), and (20) and by equations (25), (27), and (29), respectively, are two-point boundary value problems. The numerical technique used here to solve them is the Newton-Raphson method, which has enjoyed wide use in pulsation calculations (see Winget 1981; Carroll 1981). Because of the presence of internal surfaces of discontinuity in the unperturbed stellar model, however, the solution of the neutron star problem requires special procedures, which we describe below.

The solution of a general system of first-order linear equations by the Newton-Raphson method proceeds as follows. The equations can evidently be written in the form:

$$\frac{dy_i}{dx} = f_i(\{y_j\}; \Omega^2), \qquad i = 1, \ldots, I, \tag{A1}$$

where x is the independent variable, and Ω^2 is the dimensionless eigenfrequency (eq. [15]) to be determined. To complete the specification of the problem, I boundary conditions and one normalization condition are needed; these can be written in the form

$$g_l[\{y_j(a)\} \quad \text{or} \quad \{y_j(b)\}; \Omega^2] = 0, \qquad l = 1, \ldots, I+1, \tag{A2}$$

where $x = a$ and $x = b$ are the endpoints of the range of x. Equation (A1) is next cast in finite difference form, and a solution $(\{y_i\}, \Omega^2)$ is written as the sum of a trial value $(\{\bar{y}_i\}, \bar{\Omega}^2)$ plus a correction, i.e., $y_i = \bar{y}_i + \delta y_i$ and $\Omega^2 = \bar{\Omega}^2 + \delta(\Omega^2)$. Equations (A1) and (A2) are then linearized in the corrections to produce a system of algebraic equations for the corrections δy_i and $\delta(\Omega^2)$ which can be solved in terms of $\bar{y}_i$ and $\bar{\Omega}^2$. Application of the corrections yields new trial values of y_i and Ω^2, and iterations of this procedure are, in our calculations, continued until all the convergence parameters ϵ_i are less than 10^{-8}. Here the convergence parameters are defined by

$$\epsilon_i = \frac{\sum_{n=1}^{N} |\delta y_i^n|}{\sum_{n=1}^{N} |y_i^n|}, \qquad i = 1, \ldots, I, \tag{A3}$$

where N is the total number of shells. Typically, four to five iterations are required to obtain the indicated level of convergence, and at the last iteration it is not uncommon to find values of $\delta(\Omega^2)$ ranging from 10^{-22} to 10^{-25}.

For a completely fluid star, the system (A1) is the second-order equation set (eq. [18a]–[18b]). The boundary conditions are (i) regularity of the solution at the stellar center (eq. [19a]), (ii) the condition $\delta p/p \to 0$ at the stellar surface (eq. [19b]), and (iii) the normalization condition at the stellar surface (eq. [19c]). Solution of this system of equations proceeds in the following way. Between the first and second shell in the stellar model, there are five unknown quantities: the corrections δy_1 and δy_2 at the central shell, the corresponding corrections at shell 2, and the correction $\delta(\Omega^2)$ to the eigenvalue. Equation (A1) in finite difference form provides two relations among these variables, and the central boundary condition provides a third. Application of these conditions permits the elimination of three of the unknowns in terms of the remaining two. Between shells 2 and 3, we add two new unknowns, the corrections δy_1 and δy_2 at shell 3, and two new finite difference equations of the form (A1) relating those variables to the unknowns remaining at shell 2. Again the system can be solved in terms of two remaining unknowns. Evidently this process can be repeated until the shell added is the one at the stellar surface. At this point, in addition to two unknowns and two new finite difference equations, we add the surface boundary condition and the normalization condition. The system now becomes determinate, and the equation set can be solved to obtain all of the required corrections.

In the case of a neutron star with a solid crust, which we take to have an inner boundary at shell I_- and an outer boundary at shell I_+, the solution of the equation set proceeds in exactly this same way until the inner boundary of the crust is reached. In the step from shell $I_- - 1$ to shell I_-, we change from the two Dziembowski variables (eq. [16]) y_1 and y_2 to the four z-variables (eq. [11]). The variables z_1 and z_2 are related to y_1 and y_2 through the interfacial jump conditions (eq. [20a], [20b]), and the quantity $z_4 = 0$, because we impose the free slip condition (eq. [20c]) at the boundary. Thus in moving from shell $I_- - 1$ to shell I_-, we add four unknowns (the corrections δz_i at shell I_-) to the two unknowns δy_1 and δy_2 at shell $I_- - 1$, and we add three relations among these unknowns. After the application of these three relations, there remain three unknowns at shell I_-. The step from shell I_- to shell $I_- + 1$ adds four new unknowns δz_i and four relations of the form of equation (A1) among them. Clearly, in a manner similar to that of the fluid case described above, this permits the propagation of three unknown corrections through the crust to the outermost shell of the crust, I_+. At this point we must return to the Dzembowski variables in the fluid ocean. The step from shell I_+ to $I_+ + 1$ thus adds two new unknowns, the two corrections δy_i at shell $I_+ + 1$, to the three at shell I_+, together with three relations among them (the expressions relating y_1 and y_2 to z_1 and z_2 and the free slip condition $z_4 = 0$). Thus at shell $I_+ + 1$ we return to a system containing only two unknown corrections, and the remainder of the numerical solution proceeds as discussed above.

We began the testing of our numerical method using a simplified version of the code, which was designed for a model consisting of a fluid core and a solid crust, but with no surface fluid ocean. Our equilibrium model for these initial tests was a piecewise homogeneous model of the Earth kindly supplied to us by R. Buland of the United States Geological Survey. Our code reproduces the periods given by Buland for this model to better than one part in 10^5 for the spheroidal mode with the longest period. The agreement is slightly less good for the overtones, as one would expect, since there are fewer shells per wavelength for these modes. In addition, the eigenfunctions agree well except for some small differences in the horizontal motion in the core.

To test the "three-component" Newton-Raphson code, we have adopted a standard (fiducial) equilibrium neutron star model. This is the 0.5 $M_\odot$ model with central temperature $T_c \sim 10^7$ K from Richardson's evolutionary sequences mentioned above in § II. We have also carried out normal mode calculations for this model using a completely different numerical method than the

Newton-Raphson technique described here. In this other numerical approach, which is basically a shooting method, the full set of pulsation equations for liquid and fluid regions is integrated from the stellar center to the surface using a fourth-order, step-correcting, Runge-Kutta algorithm with cubic spline interpolation of the necessary stellar parameters. Jump conditions at interfaces are applied directly in this scheme. While highly accurate in principle, this method is somewhat difficult to implement because, in the solid crust of the model, there are two linearly independent solutions for z which must be computed separately and then later combined to obtain the final eigenfunctions. The general method used here has been reviewed by Woodhouse (1980). Briefly, it consists of phrasing the pulsation variables in terms of "minors," which are vector cross product representations of the z_i, and then disentangling the system to recover the z_i. Because of the computational complexity and cost, these methods were used only as benchmarks for the main set of calculations. Comparison of the results from the two different methods for modes with $l = 2$ generally shows quite good agreement. Most of the periods agree to within a few percent or better. There is one exception, however: the core/crust interfacial mode. The shooting method yields a period of 5.3 ms for this mode, while the relaxation technique yields 6.5 ms, a difference of almost 25%. Despite this difference, the eigenfunctions produced by the two different methods are very similar. We do not know the reason for the disagreement in period, but it seems to be unique to this interfacial mode. These types of interfacial modes (called Stoneley modes in geophysics) are often difficult to compute because of the steep gradients of eigenfunctions implied by the trapping on the interfaces and associated decoupling from the rest of the star (or Earth; see Buland and Gilbert 1984). Because the properties of this one mode are extremely sensitive to conditions in the vicinity of the interface, it is perhaps not too surprising that this case should yield results which depend upon the particular numerical method employed. Aside from this case, the agreement between the two sets of results for the other mode calculations provides confidence in the qualitative results and yields a measure of the residual error in these numerical computations. We also note that in numerical experiments in which $\mu \to 0$, the pulsation periods reduce to their pure fluid values. See McDermott (1985) for details.

The method of solution of the toroidal oscillation problem is essentially the same as that described for the spheroidal modes. This is a much simpler problem, because the toroidal modes are described by the second-order system (eq. [25]), with the free slip boundary condition (eq. [27]) imposed at the top and bottom of the crust, together with the normalization condition (eq. [28]). The numerical solution of this problem proceeds in a manner very similar to that described above for a purely fluid model.

REFERENCES

Aizenman, M. L., and Smeyers, P. 1977, *Ap. Space Sci.*, **48**, 123.
Aki, K., and Richards, P. G. 1980, *Quantitative Seismology: Theory and Methods* (San Francisco: Freeman).
Alterman, Z., Jarosch, H., and Pekeris, C. L. 1959, *Proc. Roy. Soc. London, A*, **252**, 80.
Arons, J. 1983, *Ap. J.*, **266**, 215.
Balbinski, E., and Schutz, B. F., 1982, *M.N.R.A.S.*, **200**, 43p.
Bardeen, J. W., Thorne, K. S., and Meltzer, D. W. 1966, *Ap. J.*, **145**, 505.
Baym, G., Bethe, H. A., and Pethick, C. 1971, *Nucl. Phys.*, **A175**, 225.
Baym, G., Pethick, C., and Sutherland, P. 1971, *Ap. J.*, **170**, 299.
Boriakoff, V. 1976, *Ap. J. (Letters)*, **208**, L43.
Brush, S. G., Sahlin, H. L., and Teller, E. 1966, *J. Chem. Phys.*, **45**, 2102.
Buland, R. 1981, *Ann. Rev. Earth Planet. Sci.*, **9**, 385.
Buland, R., and Gilbert, F. 1984, *J. Comp. Phys.*, **54**, 95.
Campolattaro, A., and Thorne, K. S. 1970, *Ap. J.*, **159**, 847.
Carroll, B. W., 1981, Ph.S. thesis, University of Colorado.
———. 1982, private communication.
Carroll, B. W., Zweibel, E. G., Hansen, C. J., McDermott, P. N., Savedoff, M. P., Thomas, J. H., and Van Horn, H. M. 1986, *Ap. J.*, **305**, 767.
Cordes, J. M. 1976, *Ap. J.*, **208**, 944.
———. 1981, in *IAU Symposium 95, Pulsars*, ed. W. Sieber and R. Wilebinski (Dordrecht: Reidel), p. 115.
Cowling, T. G. 1941, *M.N.R.A.S.*, **101**, 367.
Cox, J. P. 1980, *Theory of Stellar Pulsation* (Princeton: Princeton University Press).
Cutler, C., and Lindblom, L. 1987, *Ap. J.*, **314**, 234.
Douglass, D. H., and Braginski, V. B. 1979, in *General Relatively: An Einstein Centenary Survey*, ed. S. W. Hawking and W. Israel (Cambridge: Cambridge University Press), p. 90.
Finn, L. S. 1987, *M.N.R.A.S.*, **227**, 265.
Flowers, E. G., and Itoh, N. 1976, *Ap. J.*, **206**, 218.
Friman, B. L., and Maxwell, O. V. 1979, *Ap. J.*, **232**, 541.
Glass, E. N., and Lindblom, L. 1983, *Ap. J. Suppl.*, **53**, 93.
Gudmundsson, E. H. 1981, licentiate thesis, University of Copenhagen.
Gudmundsson, E. H., Pethick, C. J., and Epstein, R. I. 1983, *Ap. J.*, **272**, 286.
Hansen, C. J., and Cioffi, D. F. 1980, *Ap. J.*, **238**, 740.
Hansen, C. J., and Van Horn, H. M. 1979, *Ap. J.*, **233**, 253.
Ipser, J. R., and Thorne, K. S. 1973, *Ap. J.*, **181**, 181.
Jackson, J. D. 1975, *Classical Electrodynamics* (New York: Wiley).
Johnson, W. 1982, private communication.
Jones, P. B. 1981, *M.N.R.A.S.*, **197**, 1103.
———. 1982, *M.N.R.A.S.*, **200**, 1081.
———. 1984, *M.N.R.A.S.*, **209**, 569.
Joss, P. C., and Rappaport, S. A. 1984, *Ann. Rev. Astr. Ap.*, **22**, 537.
Landau, L. D., and Lifshitz, E. M. 1970, *Theory of Elasticity* (Oxford: Pergamon).
Lapwood, E. R., and Usami, T. 1981, *Free Oscillations of the Earth* (London: Cambridge University Press).
Lewin, W. H. G., and Joss, P. C. 1984, in *Accretion Driven Stellar X-Ray Sources*, ed. W. H. G. Lewin and E. P. J. van den Heuvel (Cambridge: Cambridge University Press), p. 41.
Lewin, W. H. G., and van Paradijs, J. 1986, *Comments Ap.*, **11**, 127.
Lindblom, L., and Detweiler, S. L. 1983, *Ap. J. Suppl.*, **53**, 73.
Livio, M. 1982, *Ap. Space Sci.*, **82**, 167.
Livio, M., and Bath, G. T. 1982, *Astr. Ap.*, **116**, 286.
Manchester, R. N., and Taylor, J. H. 1977, *Pulsars* (San Francisco: Freeman).
Maxwell, O. V. 1978, Ph.D. thesis, SUNY-Stony Brook.
McDermott, P. N. 1985, Ph.D. thesis, University of Rochester.
McDermott, P. N., Hansen, C. J., Van Horn, H. M., and Buland, R. 1985, *Ap. J. (Letters)*, **297**, L37.
McDermott, P. N., Savedoff, M. P., Van Horn, H. M., Zweibel, E. G., and Hansen, C. J. 1984, *Ap. J.*, **281**, 746.
McDermott, P. N., and Taam, R. E. 1985, *Bull. AAS*, **17**, 849.
———. 1987, *Ap. J.*, **318**, 278.
McDermott, P. N., Van Horn, H. M., and Scholl, J. F. 1983, *Ap. J.*, **268**, 837.
Meltzer, D. W., and Thorne, K. S. 1966, *Ap. J.*, **145**, 514.
Muhlschlegel, B. 1959, *Zs. Phys.*, **155**, 313.
Negele, J. W. 1974, in *Physics of Dense Matter*, ed. C. J. Hansen (Dordrecht: Reidel), p. 1.
Negele, J. W., and Vautherin, D. 1973, *Nucl. Phys.*, **A207**, 298.
Osaki, Y., and Hansen, C. J. 1973, *Ap. J.*, **185**, 277.
Pandharipande, V. R., Pines, D., and Smith, R. A. 1976, *Ap. J.*, **208**, 550.
Papaloizou, J., and Pringle, J. E. 1978, *M.N.R.A.S.*, **182**, 423.
Pekeris, C. L., Alterman, Z., and Jarosch, H. 1962, *Proc. Nat. Acad. Sci. US*, **48**, 5922.
Richardson, M. B. 1980, Ph.D. thesis, SUNY-Albany.
Richardson, M. B., Van Horn, H. M., Ratcliff, K. F., and Malone, R. C. 1982, *Ap. J.*, **255**, 624.
Ruderman, M. A. 1968, *Nature*, **218**, 1128.
———. 1970, *Nature*, **225**, 619.
Ruderman, M. A., and Sutherland, P. G. 1975, *Ap. J.*, **196**, 51.
Sadeh, D., and Livio, M. 1982, *Ap. J.*, **258**, 770.
Saio, H. 1982, *Ap. J.*, **256**, 717.
Sawyer, R. F. 1980, *Ap. J.*, **237**, 187.
Scalapino, D. J. 1972, *Phys. Rev. Letters*, **29**, 386.
Schumaker, B. L., and Thorne, K. S. 1983, *M.N.R.A.S.*, **203**, 457.
Smith, F. G. 1977, *Pulsars* (Cambridge: Cambridge University Press).
Taylor, J. H., and Manchester, R. N. 1977, *Ann. Rev. Astr. Ap.*, **15**, 19.
Thorne, K. S. 1969, *Ap. J.*, **158**, 1.
———. 1977, *Ap. J.*, **212**, 825.
Thorne, K. S., and Campolattaro, A. 1967, *Ap. J.*, **149**, 591.

Unno, W., Osaki, T., Ando, H., and Shibahashi, H. 1970, *Nonradial Oscillations of Stars* (Tokyo: Tokyo University Press).
Van Horn, H. M. 1980, *Ap. J.*, **236**, 899.
Van Horn, H. M., and Savedoff, M. P. 1976, in *Solar and Stellar Pulsations*, ed. A. N. Cox and R. G. Deupree (Los Alamos Report LA-6544-C), p. 109.
Winget, D. E. 1981, Ph.D. thesis, University of Rochester.
Woodhouse, J. H. 1980, in *Physics of the Earth's Interior*, ed. A. M. Dziewonski and E. Boschi (New York: Elsevier), p. 127.
Wright, G. A. E., and Fowler, L. A. 1981, *Astr. Ap.*, **101**, 356.
Yang, C.-H., and Clark, J. W. 1971, *Nucl. Phys.*, **A174**, 49.

C. J. HANSEN: Department of Astrophysical, Planetary, and Atmospheric Sciences, University of Colorado, Boulder, CO 80309

P. N. McDERMOTT: Department of Physics, Albion College, Albion, MI 49224

H. M. VAN HORN: Department of Physics and Astronomy, University of Rochester, Rochester, NY 14627